

# Impact of Chinese Urbanization and Aerosol Emissions on the East Asian Summer Monsoon

ZHIHONG JIANG, FEI HUO, AND HONGYUN MA

*Key Laboratory of Meteorological Disaster of Ministry of Education, and Joint International Research Laboratory of Climate and Environment Change, Collaborative Innovation Center on Forecast and Evaluation of Meteorological Disasters, Nanjing University of Information Science and Technology, Nanjing, Jiangsu, China*

JIE SONG

*Department of Geography, Northern Illinois University, DeKalb, Illinois*

AIGUO DAI

*Department of Atmospheric and Environmental Sciences, University at Albany, State University of New York, Albany, New York, and National Center for Atmospheric Research, Boulder, Colorado*

(Manuscript received 22 August 2015, in final form 12 October 2016)

## ABSTRACT

Impacts of urbanization and anthropogenic aerosols in China on the East Asian summer monsoon (EASM) are investigated using version 5.1 of the Community Atmosphere Model (CAM5.1) by comparing simulations with and without incorporating urban land cover and/or anthropogenic aerosol emissions. Results show that the increase of urban land cover causes large surface warming and an urban frictional drag, both leading to a northeasterly wind anomaly in the lower troposphere over eastern China (EC). This weakens the southerly winds associated with the EASM and causes a convergence anomaly in southern China (SC) with increased ascent, latent heating, and cloudiness. The enhanced latent heating reinforces surface convergence and upper-level divergence over SC, leading to more northward advection in the upper level into northern China (NC) and descending between 30° and 50°N over East Asia. Cloudiness reduction, adiabatic heating, and warm advection over NC all enhance the urban heating there, together causing anomalous tropospheric warming at those latitudes over East Asia. Anthropogenic aerosols cause widespread cooling at the surface and in the troposphere over EC, which decreases the summer land–ocean thermal contrast, leading to a weakened EASM circulation with reduced moisture transport to NC. This results in wetter and drier conditions over SC and NC, respectively. When both the urbanization and anthropogenic aerosols are included in the model, aerosols' cooling is partially offset by the urban heating, and their joint effect on the circulation is dominated by the aerosols' effect with a reduced magnitude. In the combined experiment, surface and tropospheric temperatures are also altered by the decrease (increase) in cloudiness over NC (SC) with most of the cooling confined to SC, which further weakens the EASM circulation.

## 1. Introduction

Rapid urban expansion has occurred in China at an unprecedented scale in the last three decades. The urban population of China has increased by  $1.2\% \text{ yr}^{-1}$  from 1998 to 2008 (Wang 2010). In 2014, a landmark urbanization plan was unveiled with a goal to have 60% of the population living in cities by 2020, up from 54% in 2014 (National Bureau of Statistics of China 2014). Such

large-scale urbanization has been reshaping the physical environment over East Asia by converting croplands and pasture to urban area, by agglomerating supersized cities, urban clusters, and districts, and by increasing pollutants in the atmosphere. Since urban surface alters the dynamic, thermal, and hydraulic properties of the natural surface and adds anthropogenic heat to the atmosphere, it can affect surface energy and water fluxes and thus precipitation and local climate. Moreover, changes in precipitation, together with the direct impacts from urbanization, can result in regional alterations in tropospheric heating and thus in atmospheric circulation

---

Corresponding author e-mail: Zhihong Jiang, zhjiang@nuist.edu.cn

patterns (Pielke 2005). On the other hand, increased anthropogenic aerosols due to urbanization and industrialization can cool the surface by directly reflecting solar radiation and indirectly increasing the reflectivity of clouds (Albrecht 1989). They can change precipitation even in regions far away from highly polluted areas (Wang 2013). Therefore, urban land use and anthropogenic aerosols can have large impacts on regional climate.

Previous studies suggest that recent changes in land use could be of equal importance as the increase in greenhouse gases for many regions (Pielke 2005; Findell et al. 2007; Lawrence and Chase 2010) and that the complex range of effects of various human disturbances on climate need to be studied in order to understand and assess past and future climate changes (Feddesma et al. 2005). Even though land-use change is increasingly recognized as an important component for human-induced climate change, the effect of urbanization on regional climate is still quite uncertain, especially over East Asia, where large-scale urbanization may cause a dynamical adjustment of the atmosphere and could exert important influences on precipitation processes through thermodynamic feedback during the East Asian summer monsoon (EASM; Feng et al. 2015; Ma et al. 2016; Chen et al. 2016).

Observational data analyses have shown that recent large-scale urban expansion in China has contributed to surface warming (Kalnay and Cai 2003; Zhou et al. 2004; Xie et al. 2007; Jones et al. 2008; Li and Yan 2009; Dai et al. 2011). The effect of urban expansion on precipitation, however, is more complicated. It depends on the region, season, and spatial scale considered. At the local scale, by analyzing satellite land-use maps and station observations, Kaufmann et al. (2007) found that urban expansion in the Pearl River delta of China may reduce local precipitation by changing vegetation cover and water flows in ways that reduce water supplies to the local atmosphere. In contrast, several observational and modeling studies indicated that urbanization in other parts of the world significantly enhances both the intensity of storms over the urban area and the downwind rainfall by increasing surface roughness convergence and downwind shifting of urban heat island circulation (Changnon 1978; Shepherd et al. 2002; Kishtawal et al. 2010). Using ensemble simulations, Wan and Zhong (2014) investigated the impact of urban clusters in the lower reaches of the Yangtze River valley (YRV) in China on a summer precipitation event and found that precipitation started later but was stronger and that the precipitation pattern was shifted farther north because of the urban land use. In these studies, only the local urban effect near the surface was analyzed. Thus, these studies could not account for the impact of large-scale

urbanization on regional climate because the impact is well beyond near-surface heating by the urban heat island and the downwind rainfall enhancement (Zhang et al. 2009; Chen and Zhang 2013; Deng and Xu 2015).

Model sensitivity experiments have been widely used to simulate the effect of urban land use on regional climate. Several modeling studies have adopted a simplified urban parameterization approach, in which modifications were made on land surface parameters, such as albedo, roughness length, heat, and hydrologic properties. Using this simplified urban scheme, an extreme urban expansion experiment conducted by Shao et al. (2013) with a regional climate model (RegCM3) has shown that intensive urbanization in eastern China (EC) could enhance southwesterly wind in the early monsoon season but weaken it during the summer. Using a general circulation model (LMDZ) with the simplified urban scheme, Zhou et al. (2015) found that during the EASM urban land-use expansion could result in positive (negative) upper-tropospheric geopotential height anomalies in southern (northern) China and strengthen the western Pacific subtropical high (WPSH) with westward expansion. The urban land-use experiments in these studies show reduced precipitation and significant changes in the atmospheric circulation during the EASM season over eastern China, especially south of the YRV.

Other studies have used models that incorporate a sophisticated physical urban module, such as the Community Atmosphere Model (CAM) and Weather Research and Forecasting (WRF) Model. As fractions of urban land cover in coarse model grid cells are often overwhelmed by other dominant land covers in most parts of the world, many sensitivity studies have to use scenarios with elevated fractions of urban cover. Model results from intensive large-scale urbanization showed that in the spring the urbanization could weaken southwesterly winds in the lower troposphere over southern China (SC), leading to reduced moisture transport to northern China (NC) and increased air temperatures both near the surface and in the lower troposphere in northern China (Deng and Xu 2015). During the summer, urbanization could not only lead to significant warming over most of the expanded urban areas but also strengthen the summer monsoon across eastern China in early summer and weaken the monsoon over the southern part of East Asia in late summer (Chen et al. 2016).

Other model simulations used current realistic urban land use in China. They showed somewhat different results from those with idealized urban land use. Using version 5.1 of the Community Atmosphere Model (CAM5.1), Ma et al. (2016) found that current urban land

expansion weakens the EASM and causes surface warming (cooling) and precipitation decreases (increases) in northern (southern) China. This north–south opposite pattern of temperature change differs from the uniform surface warming over eastern China found by [Chen et al. \(2016\)](#), despite the fact that both showed a north–south opposite precipitation change pattern. In contrast, using the WRF Model, [Feng et al. \(2015\)](#) found that urban expansion in China slightly strengthens the EASM because of the enhanced land–sea thermal contrast and reduces summer precipitation in most urban areas in eastern China. Thus, there are still large discrepancies and even contradictions regarding the impacts of large-scale urbanization in China on summer monsoon circulation, temperature, and precipitation over East Asia. In particular, there is still a need to understand the detailed physical mechanisms responsible for the simulated climate response to urbanization in China.

Accompanying the large-scale urbanization, massive industrialization since the 1980s has made China a major source of anthropogenic aerosols as 70% of its energy comes from coal combustion ([U.S. Energy Information Administration 2012](#)). Since 1980, anthropogenic aerosol emissions have increased significantly in Asian countries, especially in China ([Streets et al. 2003](#)). Chinese coal production and sulfur emissions have increased by 2.5 times during 1980–2003, by far the largest increase in the world ([Ohara et al. 2007](#)). The annual release of  $\text{SO}_2$  in China surpassed 20 Tg (1 Tg =  $10^{12}$  g) during 1992–98 ([Xu 2001](#)), and it has increased further since 2000 ([Smith et al. 2011](#)). As a result, atmospheric aerosol optical depth (AOD) has increased steadily over East Asia since 1980 ([Li 2004](#); [Wang et al. 2011](#)).

Many studies have shown that aerosols can affect the climate in many ways ([Lohmann and Feichter 2005](#); [Rosenfeld et al. 2008](#); [Boucher et al. 2013](#); [Wang 2013](#)). Aerosols directly reflect and absorb solar radiation in the atmosphere, thus reducing solar radiation reaching the surface and altering its vertical distribution in the atmosphere. They also alter cloud properties and thus indirectly affect shortwave and longwave radiation by acting as cloud condensation nuclei and ice nuclei ([Albrecht 1989](#)). More specifically, sulfate aerosols, produced following  $\text{SO}_2$  emissions, scatter and reflect sunlight; thus, they directly cool the surface and the lower troposphere. They can also have an indirect cooling effect by increasing reflectivity of clouds. On the other hand, black carbon (BC) aerosols are a strong absorber of sunlight, thus providing a strong radiative heating in the atmosphere ([Charlson et al. 1992](#)). [Bollasina et al. \(2011\)](#) investigated the response of the South Asian summer monsoon (SASM) to natural and anthropogenic aerosol forcings and found that the

widespread summertime drying over South Asia during the second half of the twentieth century could be attributed mainly to anthropogenic aerosol emissions. There is also some empirical evidence (e.g., [Xu 2001](#)) that links the aerosols' cooling effect to the abnormal summer rainfall pattern in eastern China during 1960–99, suggesting that the increasing levels of sulfate aerosols may have significantly affected the summer climate over eastern China during recent decades. Recently, [Wu et al. \(2016\)](#) showed that cloud physical properties and precipitation may be significantly affected by aerosols in China with aerosols likely suppressing local light and moderate rainfall but intensifying heavy rainfall in southeast coastal regions of China. They called attention to the interaction between aerosols and the EASM as high moisture levels in the monsoon region could affect aerosols optical and radiative properties.

It is well known that the EASM circulation has weakened from the 1960s to 1990s (e.g., [Gong and Ho 2002](#); [Yu et al. 2004](#); [Ding et al. 2008](#); [Li et al. 2010](#); [Ding et al. 2015](#)). One wonders if the large-scale urbanization and aerosol increases since the 1980s have contributed to the recent change in EASM. Some studies analyzed observed temperature changes between land and oceans that affects monsoon activity ([Miyakoda et al. 2003](#); [Yang and Lau 2006](#); [Ding et al. 2009](#)), while other studies examined model simulations and reanalysis data ([Li et al. 2010](#); [Dai et al. 2013](#)). Based on atmospheric model experiments, [Li et al. \(2010\)](#) showed that tropical surface warming from the late 1970s to 2000, especially in the tropical central and eastern Pacific, reduces the summer land–sea thermal contrast over the Asian monsoon region and contributes to the observed weakening in EASM circulation. On the other hand, the direct effect of greenhouse gases (GHGs) was found to increase the near-surface land–sea thermal contrast and thus favors a slightly enhanced rather than weakened EASM circulation ([Li et al. 2010](#); [Song et al. 2014](#)). Moreover, the strength of Asian summer monsoons (including the EASM) was argued to be more closely coupled with the land–sea thermal contrast in the upper troposphere rather than in the lower troposphere or near the surface ([Sun et al. 2010](#); [Dai et al. 2013](#)).

Recently, [Jiang et al. \(2013\)](#) studied the effects of different types of aerosols on clouds and precipitation during EASM, using CAM5 with a coarse resolution ( $1.9^\circ$  latitude  $\times$   $2.5^\circ$  longitude). [Jiang et al. \(2013\)](#) found that anthropogenic sulfates and primary organic matter (POM) contribute the most among all anthropogenic aerosols to the cooling near the surface and in the free troposphere over land in northern China, where large values of AOD were located. This cooling suppressed precipitation in northern China but enhanced

precipitation in southern China and adjacent oceans. In comparison, anthropogenic BC aerosol-induced precipitation changes are statistically insignificant. Jiang et al. (2013) also noted that the simulated cooling is larger in northern China than in southern China, which seems to be inconsistent with the observations that show a large cooling in the YRV and southern China and a moderate warming in northern China (Xu et al. 2006). Although the observations include many other effects, the difference in the modeled and observed cooling regions cannot simply be explained by the exclusion of the increased GHGs in their simulations. This is because aerosols' negative radiative forcing is stronger than GHGs' positive forcing during the summer over China (Xu 2001). To examine the contributions of different forcings to the weakening of the EASM circulation, Song et al. (2014) analyzed results from phase 5 of the Coupled Model Intercomparison Project (CMIP5) models and showed that the weakening of the EASM circulation was only partly captured in the multimodel ensemble mean under natural (solar and volcanic) and anthropogenic (GHGs and aerosols) forcings, but the ensemble failed to simulate the "southern flood and northern drought pattern," as found in other modeling studies (e.g., Li et al. 2010). The cooling effect of aerosols and the weakening of the EASM circulation were seen among most modeling studies; however, there are discrepancies in response of temperature and precipitation, and physical mechanisms that produced these responses were not fully understood. Therefore, further investigations are needed to understand the effect of anthropogenic aerosols on the EASM circulation and on temperature and precipitation over East Asia.

As discussed above, model simulations with idealized (e.g., Deng and Xu 2015; Chen et al. 2016) and realistic (e.g., Ma et al. 2016) urbanizations over China have been conducted to study possible responses of East Asian climate. Other numerical studies have also been carried out to investigate aerosols' effects on East Asian climate (e.g., Jiang et al. 2013; Song et al. 2014). However, few studies have compared the individual effects of the urban land use and anthropogenic aerosols and examined their combined effects on East Asian climate. The purpose of this study is to investigate the impacts of recent urban land use and anthropogenic aerosols in China, separately and jointly, on large-scale EASM circulation and regional climate, with a focus on understanding the feedback mechanisms that induce and maintain the large-scale changes. In comparison with previous studies, more detailed physical mechanisms for the simulated climate responses to urban land cover and aerosols are examined in the study. The paper is organized as follows. In section 2, the model and numerical

experiments are described. The main results and the physical mechanisms are presented in sections 3 and 4, respectively. A summary and conclusions are presented in section 5.

## 2. Model and experiments

### a. Model description

In this study, model simulations were conducted using CAM5.1, the atmospheric component of the Community Earth System Model, version 1 (CESM1; Neale et al. 2012). CAM5.1 has been improved considerably in almost all physical parameterizations in comparison with its previous version (Neale et al. 2012). It has shown significant improvements in precipitation simulations by implementing a physically based two-moment microphysics parameterization scheme for convective clouds that enables their interaction with large-scale clouds and aerosols (Song et al. 2012). In addition to simulating the direct radiative effects of aerosols, the physical parameterization enhancements make it possible to simulate full aerosol–cloud interactions, which include cloud droplet activation by aerosols, precipitation processes due to particle-size-dependent behavior, and the explicit radiative effect of cloud particles.

A modal aerosol module (MAM) has been developed for CAM5.1 (Liu et al. 2012). It enables the approximate simulation of the aerosol size distribution, internal and external mixing between aerosol components, numerous aerosol processes, and aerosol physical, chemical, and optical properties in a physically based manner. For the purpose of this study, the three-mode MAM (MAM3) option, which includes Aitken, accumulation, and coarse modes, was chosen to simulate the properties and processes of major aerosol species in the atmosphere, such as sulfate and BC aerosols, primary organic matter, secondary organic aerosols, mineral dust, and sea salt (Liu et al. 2012). The size distribution of each mode was assumed to be lognormal. Aerosol particles that were suspended in the air and attached to (or contained within) different hydrometeors, such as cloud droplets, were explicitly predicted. The CAM5.1 model used here employed the finite-volume and semi-Lagrangian scheme and had 30 layers in an eta vertical coordinate with the model top at 3.6 hPa. The model integrated explicitly with a 30-min time step.

CAM5.1 is coupled with the Community Land Model, version 4.0 (CLM4.0; Oleson et al. 2010a). Model grid cells for the land surface are composed of multiple land units to capture the spatial heterogeneity of the land surface. Urban land use is one of those land units represented. An urban canyon model [Community Land

TABLE 1. Modeling experiments: present-day land-use data collected in the early 2000s and aerosol emission data published in 2000 for the three preindustrial scenarios, changes are made only in the domain of 20°–50°N, 100°–125°E (Fig. 1) for NoU, NoA, and NoUA.

Experiment	Urban land cover	Aerosol emissions
CTL	Yes	Yes
NoU	No	Yes
NoA	Yes	No
NoUA	No	No

Model Urban (CLMU)] is integrated into CLM4.0 to contrast urban and rural energy budget and climate (Oleson et al. 2010b). CLMU is a physically based model designed to represent physical processes over an urban area known to influence regional climate. The parameterization scheme for roof, wall (shaded and unshaded), and ground (permeable and impermeable) enables a realistic simulation of land–atmosphere exchanges in momentum, heat, and water vapor over an urban region (Oleson et al. 2008). For instance, the arrangement of large roughness elements such as buildings and trees increases the frictional drag of the surface on atmospheric winds and thus reduces the mean wind speed and turbulent mixing within the urban canopy compared to more open rural areas (Oke 1987). The anthropogenic source of heat such as waste heat from building heating and cooling is also included explicitly in the urban energy budget. In CLMU, urban columns interact with one another through multiple exchanges of shortwave and longwave radiation. The heat and moisture fluxes from each surface influence each other through a bulk air mass approach in which temperature and specific humidity are predicted.

For CLM4.0, present-day land-cover type and distribution data were developed based on a variety of satellite products in the early 2000s (Oleson et al. 2010a). Present-day urban extent and properties were developed by Jackson et al. (2010) based on LandScan 2004, and a global population density dataset was derived from census data, nighttime light satellite observations, road proximity, and slope in 2004. Thus, the present-day land and urban data used here are for the year 2004. It is worth mentioning that anthropogenic heating associated with urban land use is included in the energy budget calculation in CLMU; therefore, the effect of urban land use in this paper has the effect of anthropogenic heating.

In CAM5.1, natural and anthropogenic emission rates for aerosols and precursor gases are controlled by the input data separately, and the spatial distribution and radiative forcing of the aerosols are explicitly modeled inside CAM5.1. Emissions of anthropogenic aerosols

and precursor gases, including SO<sub>2</sub>, POM, and BC for present-day and preindustrial times, were based on an inventory dataset for the years 2000 and 1850, respectively, which were produced by Lamarque et al. (2010) in support of the climate modeling research for the Intergovernmental Panel on Climate Change (IPCC) Fifth Assessment Report (AR5).

### b. Experiment design

Here we investigate the impacts of both urban land-use change and anthropogenic aerosols on the EASM by using a finer-resolution (0.9° latitude × 1.25° longitude) CAM5.1. We used observed monthly SSTs and sea ice concentration (Hurrell et al. 2008) for the ocean boundary condition in the model simulations. All of our experiments were performed over a 20-yr period from January 1988 to December 2007 with CO<sub>2</sub> level fixed at 367 ppm. Land use and anthropogenic aerosol emissions were specified at the preindustrial and present-day levels in two contrasting experiments. Results of the last 15 yr (1993–2007) were analyzed for June, July, and August (JJA).

Because atmospheric and surface heating dominates the land–sea thermal contrast for the EASM, and atmospheric and near-surface responses to changes in the urban land use and anthropogenic aerosols are much faster than oceanic processes, it is reasonable to force CAM5.1 with prescribed SSTs (instead of coupling it to an ocean GCM). This limits the response and feedback from the oceans in our experiments. Since we used the same SST forcing in our experiments, the impact of the SST changes from 1993 to 2007 is largely removed by looking at the differences between the two experiments, although it is possible to examine SST's impact by examining the year-to-year variations (but this is not done here). Here we focus on the impacts of changing urban land cover and anthropogenic aerosols, separately and jointly, on the EASM.

Table 1 summarizes the four experiments performed in this study. The control experiment (CTL) simulates the present-day (for year 2004) climate, with present-day global land-use distribution and emission rates of both natural and anthropogenic aerosols as input data. The NoU experiment is the same as CTL except there is no urban land cover over eastern China. The urban land type of CTL in each grid cell was replaced in the NoU experiment by the dominant land-use category (excluding urban land cover) in that grid cell over eastern China only (i.e., this change was made only inside the outlined box shown in Fig. 1); other land-cover types over eastern China and the urban land cover outside eastern China were kept at the present-day condition (i.e., the same as in CTL). The primary vegetation types used to

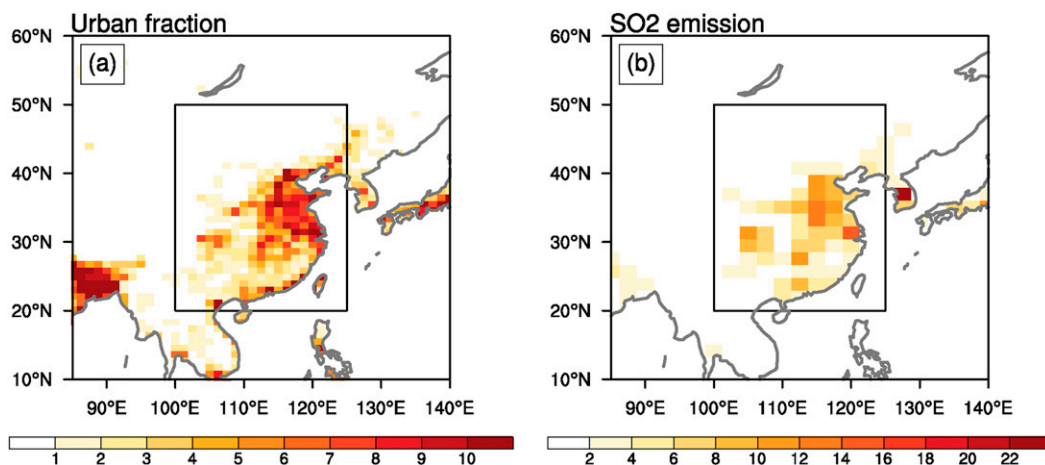


FIG. 1. (a) Distribution of urban land-cover fraction (% of CAM5.1 gridcell area) and (b) anthropogenic  $\text{SO}_2$  emissions ( $10^9$  molecules  $\text{cm}^{-2} \text{s}^{-1}$ ) used in the control experiment (CTL). The present-day land-use data were collected in the early 2000s and aerosol emission data are for year 2000. The  $\text{SO}_2$  emission patterns are representative of anthropogenic emissions for all the other aerosols and precursor gases. The values in the framed region ( $20^\circ\text{--}50^\circ\text{N}$ ,  $100^\circ\text{--}125^\circ\text{E}$ ) are set to zero in the experiments for NoU, NoA, and NoUA, respectively, with values outside the outlined box being the same as in CTL.

replace the urban area are mostly pasture grass, crops, or forest. The difference between CTL and NoU (CTL – NoU) represents the effect of urban land use over eastern China on Asian climate. The NoA experiment is the same as CTL except there is no anthropogenic aerosol emissions from eastern China. Aerosol emissions over eastern China were set to their preindustrial levels for year 1850 when only natural emissions existed (but aerosol emissions outside eastern China were set to the present-day levels). The difference between CTL and NoA (CTL – NoA) represents the effect of anthropogenic aerosols from eastern China. In the NoUA experiment, both the urban land use and anthropogenic aerosol emissions were absent over eastern China (but were at the present-day values for other regions), and its difference from CTL (CTL – NoUA) reflects the combined effects of urban land use and anthropogenic aerosol emissions in eastern China. We emphasize that our experiments were designed to simulate the mean impacts of the present-day urbanization and aerosols on Asian climate relative to preindustrial conditions. Our results are relevant to recent climate changes over China as these impacts likely contributed to the recent climate changes together with other climate forcings (e.g., GHGs) and natural climate variability [e.g., the interdecadal Pacific oscillation (IPO); Dong and Dai 2015].

The present-day urban land use and anthropogenic aerosol emissions used in CTL are illustrated in Fig. 1, in which the  $\text{SO}_2$  emission patterns are representative of all other anthropogenic aerosols and precursor gases. Figure 1 shows that both fractional coverage of urban land use and emissions of anthropogenic aerosols have

become considerable in eastern China. The region with the largest urban fractional coverage ( $>5\%$  of the CAM5.1 grid cell) is mostly in northern China and the YRV, where high aerosol emission rates are also seen. Thus, in the three sensitivity experiments, changes in urban land use (referred to as “urban”) and anthropogenic aerosol and precursor gas emissions (referred to as “aerosol”) were made over eastern China within the region of  $20^\circ\text{--}50^\circ\text{N}$ ,  $100^\circ\text{--}125^\circ\text{E}$  (Fig. 1), while no changes were made outside this region in order to isolate the impacts from this region alone.

### 3. Experiment results

#### a. Evaluation of simulations

Many studies have evaluated the performance of CAM5 (e.g., Liu et al. 2012). Here we present a general comparison of the spatial variations between model output from CTL and observations (or reanalysis) at both global and regional scales for JJA during 1993–2007 (Table 2). The observational data for 2-m air temperature were obtained from the Climatic Research Unit (CRU; Harris et al. 2014), and the precipitation data were from the Global Precipitation Climatology Project, version 2 (GPCP; Adler et al. 2003; Huffman et al. 2009). The reanalysis data for geopotential height and horizontal winds at 850 and 200 hPa were from ERA-Interim (Dee et al. 2011). Because the values of these time-varying fields may not be independent among some nearby grid points, a measure to calculate the effective number of spatial degrees of freedom (ESDOF) is utilized for these fields, following Bretherton et al.

TABLE 2. The spatial correlation coefficients between simulations and observations for JJA averaged over 1993–2007 for precipitation rate (precip), surface air temperature at 2 m (T2m), geopotential height (Z), and zonal (U) and meridional (V) wind components at 200, 500, and 850 hPa. The observation data for T2m were from CRU, and the precipitation data were from GPCP version 2. The reanalysis data for geopotential height and horizontal wind at 850 and 200 hPa were from ERA-Interim. The domain for East Asia is 20°–60°N, 110°–140°E. The threshold correlation with different effective number of spatial degrees of freedom for statistical significance at the 5% level is given in parentheses.

Domain	Surface						200 hPa					
	Precip	T2m	Z850	U850	V850		Z500	U500	V500	Z200	U200	V200
Global	0.603 (0.062)	0.943 (0.062)	0.986 (0.062)	0.990 (0.074)	0.788 (0.098)		0.997 (0.062)	0.991 (0.062)	0.847 (0.217)	0.901 (0.062)	0.975 (0.062)	0.868 (0.142)
East Asia	0.582 (0.444)	0.964 (0.174)	0.982 (0.088)	0.980 (0.553)	0.861 (0.273)		0.989 (0.217)	0.931 (0.444)	0.741 (0.468)	0.981 (0.235)	0.964 (0.312)	0.665 (0.413)

(1999). To compare the spatial variations between model output from CTL and observations (or reanalysis), the statistical significance of pattern correlations between observations (or reanalysis) and the CTL experiment is evaluated using Student's *t* test against a null hypothesis that variations between the model output and observations at all grid points are uncorrelated.

Figures 2a–d compare the 1993–2007 mean summer near-surface air temperature and precipitation in East Asia from observations and the CTL experiment. The model reasonably simulates the temperature distribution, which gradually decreases from the southeast coast of China to the northwest inland (Fig. 2a). The pattern correlation between the simulated and observed temperature fields is very high at 0.96 over East Asia (Table 2), although the simulated temperature over the northern Tibetan Plateau is higher than the observed (Fig. 2b). The comparison with the GPCP precipitation indicates that the model can simulate the general patterns of summer rainfall over East Asia ( $r = 0.58$ ), which gradually decreases from southeastern to northwestern China (Fig. 2c). Southeastern China lies next to the steep edge of the Tibetan Plateau (30°–35°N, 100°–105°E), where the difference of precipitation between CTL and GPCP is up to 6 mm day<sup>-1</sup> (Fig. 2d). The wet bias reveals shortcomings of the physical schemes used. Yu et al. (2015) found that the semi-Lagrangian advection method incorporated into CAM5.1 can easily cause an incorrect steady solution when the model is topographically forced with a large time step and wind speed. On the other hand, the model can capture the main features of the Asian summer monsoon circulations: westerly winds at 850 hPa prevail over Southeast Asia, and southwesterly winds transport moisture from the Indian Ocean to East Asia (Fig. 2e). However, the model simulates a northward shift of WPSH, which leads to stronger low-level southwesterlies at 850 hPa (Fig. 2f). In addition, a positive bias in 200-hPa geopotential height is found over northeastern China (Fig. 2h), which causes a weak westerly flow between 30° and 40°N. Despite these differences, the correlation coefficients for JJA geopotential height at 850 and 200 hPa are greater than 0.78, which is statistically significant at the 5% level with 22 060 (500) and 1442 (67) ESDOF for the global (East Asian) domain, respectively (Table 2). Comparisons between the simulated and observed temperature, precipitation, and winds indicate that over most of East Asia, the model can simulate the prominent features of the atmospheric thermodynamic states and the EASM circulation, though the biases are large, especially in precipitation (Fig. 2). It is assumed that the biases are approximately constant between CTL and sensitivity simulations.

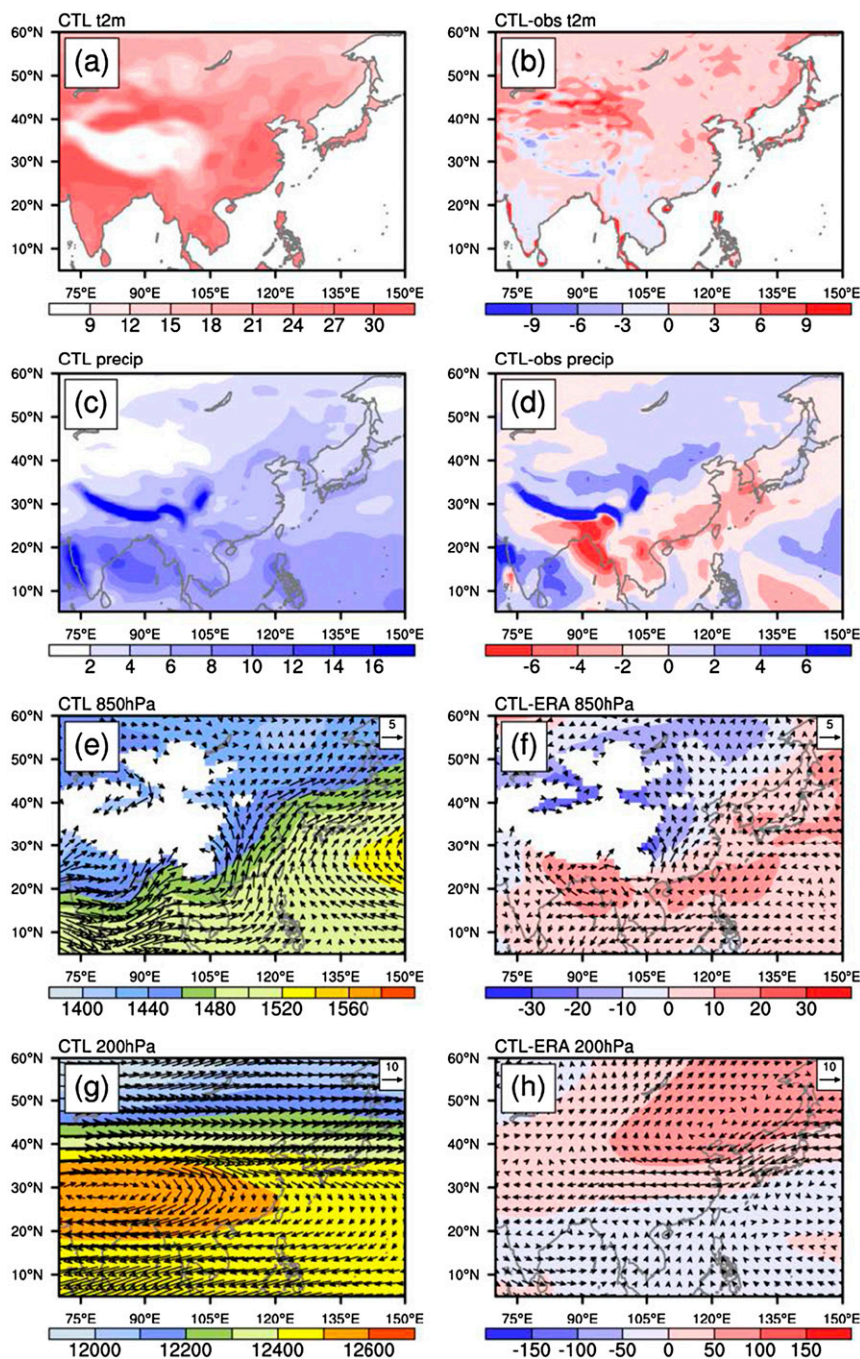


FIG. 2. The 1993–2007 mean JJA (a),(b) surface air temperature ( $^{\circ}\text{C}$ ); (c),(d) total precipitation ( $\text{mm day}^{-1}$ ); and geopotential height (m; color) and winds ( $\text{m s}^{-1}$ ; vectors) at (e),(f) 850 and (g),(h) 200 hPa over Asia. (a),(c),(e),(g) The CTL experiment and (b),(d),(f),(h) differences between the CTL experiment and the observations/ERA-Interim.

Hence, the difference between CTL and sensitivity simulations (e.g., CTL – NoU) should be effectively controlled for biases.

To investigate the effects of the urban and/or aerosol changes on regional climate, examination is first focused on surface temperature, precipitation, and

variables that are most directly associated with them—namely, AOD, total cloudiness, and surface net shortwave radiation (referred to as shortwave radiation) for clear sky and all sky. To facilitate the analysis, the main regions influenced by the EASM are delineated geographically as EC ( $20^{\circ}$ – $45^{\circ}\text{N}$ ,  $105^{\circ}$ – $122^{\circ}\text{E}$ ), which

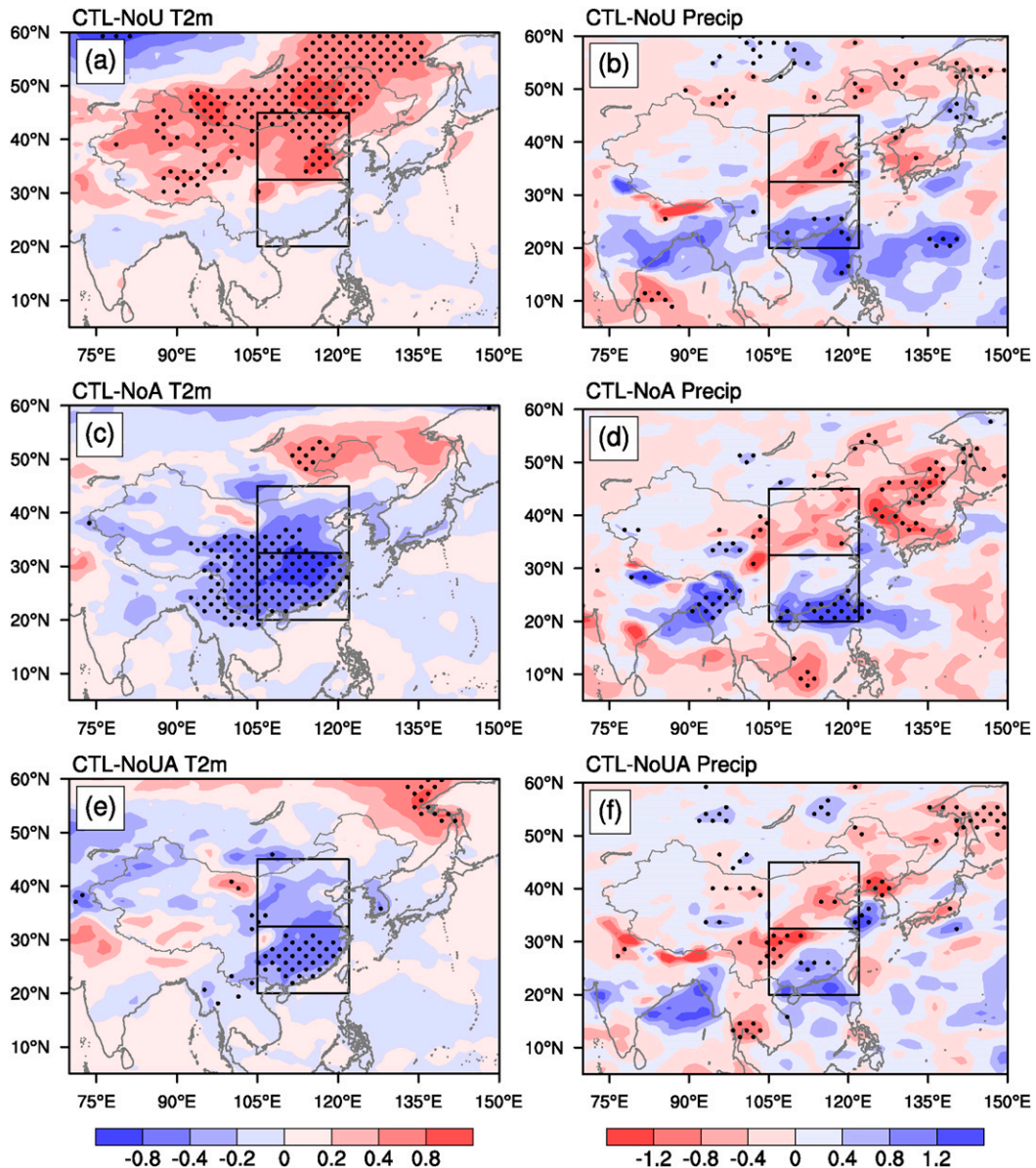


FIG. 3. Changes of the summer (left) surface air temperature ( $^{\circ}\text{C}$ ) and (right) precipitation ( $\text{mm day}^{-1}$ ) for (a),(b) CTL – NoU; (c),(d) CTL – NoA; and (e),(f) CTL – NoUA. The dotted areas are statistically significant at the 10% level. The black outlines indicate the three regions chosen for study: EC ( $20^{\circ}$ – $45^{\circ}\text{N}$ ,  $105^{\circ}$ – $122^{\circ}\text{E}$ ), NC ( $32.5^{\circ}$ – $45^{\circ}\text{N}$ ,  $105^{\circ}$ – $122^{\circ}\text{E}$ ), and SC ( $20^{\circ}$ – $32.5^{\circ}\text{N}$ ,  $105^{\circ}$ – $122^{\circ}\text{E}$ ) in Table 3.

includes SC ( $20^{\circ}$ – $32.5^{\circ}\text{N}$ ,  $105^{\circ}$ – $122^{\circ}\text{E}$ ) where the mid-to lower YRV ( $28^{\circ}$ – $31.5^{\circ}\text{N}$ ,  $113^{\circ}$ – $122^{\circ}\text{E}$ ) is enclosed, and NC ( $32.5^{\circ}$ – $45^{\circ}\text{N}$ ,  $105^{\circ}$ – $122^{\circ}\text{E}$ ), which covers northern China, the Huai River basin, the mid-to-lower Yellow River basin (YRB), and the Shandong Peninsula. The outlines of the NC and SC regions are illustrated in Fig. 3. To facilitate the comparison of the impacts of the urban and/or aerosol changes over these regions, changes in EASM-relevant quantities averaged over each of the regions are summarized in Table 3, which

serves as a guidance and reference in the following discussions.

#### b. Surface temperature and precipitation changes

The surface air temperature and precipitation changes induced by the urban and/or aerosol changes are shown in Fig. 3. The urban land use results in significant surface warming of  $0.6^{\circ}$ – $1.0^{\circ}\text{C}$  over NC where fractional urban land cover is relatively high (Fig. 3a). Significant warming also occurs in regions to the northwest and

TABLE 3. Changes in the EASM-relevant quantities that are influenced by urban land use and anthropogenic aerosols. The quantities include (a) surface air temperature at 2 m (T2m); (b1) precipitation (Precip); (b2) convective precipitation (Precip\_conv); (b3) non-convective precipitation (Precip\_non-conv); (c1) surface net radiation (Rnet); (c2) sensible (SH) and (c3) latent heat (LH) fluxes; (d) AOD; the amount of (e1) total, (e2) high, and (e3) low cloud; net shortwave radiation at top of the atmosphere (TOA) for (f1) clear sky (Snet\_clear\_TOA) and (f2) all sky (Snet\_total\_TOA); net shortwave radiation at surface for (f3) clear sky (Snet\_clear\_surf) and (f4) all sky (Snet\_total\_surf); (g) sea level pressure (SLP); (h1) geopotential height at 500 hPa ( $Z_{500}$  hPa); (h2) vertical velocity at 500 hPa; (i) 200-hPa zonal wind ( $U_{200}$  hPa); (j) atmospheric stability at 900 hPa; and (k) CAPE. Their differences between the experiments were averaged over EC (20°–45°N, 105°–122°E), NC (32.5°–45°N, 105°–122°E), and SC (20°–32.5°N, 105°–122°E). The numbers in boldface are statistically significant at the 10% level.

	CTL – NoU			CTL – NoA			CTL – NoUA		
	EC	NC	SC	EC	NC	SC	EC	NC	SC
(a) T2m (°C)	<b>0.33</b>	<b>0.60</b>	0.05	<b>-0.51</b>	-0.41	<b>-0.63</b>	<b>-0.36</b>	-0.33	<b>-0.39</b>
(b1) Precip (mm day <sup>-1</sup> )	0.09	-0.28	0.49	0.14	-0.34	<b>0.67</b>	-0.02	-0.25	0.22
(b2) Precip_conv (mm day <sup>-1</sup> )	0.07	-0.16	0.32	0.03	<b>-0.26</b>	0.35	-0.01	-0.22	0.21
(b3) Precip_non-conv (mm day <sup>-1</sup> )	0.02	-0.12	0.16	0.11	-0.08	<b>0.33</b>	-0.01	-0.03	0.01
(c1) Rnet (W m <sup>-2</sup> )	1.07	<b>6.09</b>	-4.35	<b>-15.91</b>	<b>-11.34</b>	<b>-20.83</b>	<b>-14.15</b>	<b>-11.16</b>	<b>-17.37</b>
(c2) SH (W m <sup>-2</sup> )	1.32	<b>2.53</b>	0.02	<b>-4.23</b>	<b>-2.15</b>	<b>-6.48</b>	<b>-3.94</b>	<b>-2.60</b>	<b>-5.39</b>
(c3) LH (W m <sup>-2</sup> )	-1.03	-0.18	<b>-1.93</b>	<b>-5.35</b>	<b>-5.56</b>	<b>-5.12</b>	<b>-5.31</b>	<b>-4.88</b>	<b>-5.78</b>
(d) AOD	-0.01	-0.01	-0.01	<b>0.09</b>	<b>0.10</b>	<b>0.07</b>	<b>0.09</b>	<b>0.10</b>	<b>0.07</b>
(e1) Total cloud (%)	-0.43	-1.79	1.05	0.99	-0.55	2.64	1.44	-0.10	3.10
(e2) High cloud (%)	-0.51	-1.90	0.99	0.54	-1.26	2.48	1.12	-0.70	3.08
(e3) Low cloud (%)	-0.19	-1.30	1.01	1.40	0.62	<b>2.22</b>	0.78	0.26	1.31
(f1) Snet_clear_TOA (W m <sup>-2</sup> )	-0.14	0.01	<b>-0.30</b>	<b>-1.59</b>	<b>-1.79</b>	<b>-1.38</b>	<b>-1.86</b>	<b>-1.87</b>	<b>-1.86</b>
(f2) Snet_total_TOA (W m <sup>-2</sup> )	-0.54	3.44	-4.83	<b>-9.54</b>	<b>-4.30</b>	<b>-15.18</b>	<b>-8.42</b>	<b>-4.49</b>	<b>-12.65</b>
(f3) Snet_clear_surf (W m <sup>-2</sup> )	-0.15	0.10	-0.43	<b>-7.42</b>	<b>-8.42</b>	<b>-6.34</b>	<b>-7.83</b>	<b>-8.60</b>	<b>-7.01</b>
(f4) Snet_total_surf (W m <sup>-2</sup> )	-0.48	3.91	-5.21	<b>-15.12</b>	<b>-10.40</b>	<b>-20.21</b>	<b>-13.93</b>	<b>-10.57</b>	<b>-17.56</b>
(g) SLP (Pa)	-20.03	-17.92	-22.32	42.81	<b>53.37</b>	31.44	6.76	10.60	2.62
(h1) $Z_{500}$ hPa (m)	<b>-5.29</b>	0.11	<b>-8.92</b>	-1.27	-2.89	0.47	-1.89	0.01	<b>-3.49</b>
(h2) 500 hPa vertical velocity (10 <sup>-3</sup> Pa s <sup>-1</sup> )	-0.02	3.00	-3.27	-1.44	3.57	<b>-6.83</b>	-0.25	1.81	-2.47
(i) $U_{200}$ hPa (m s <sup>-1</sup> )	-0.62	<b>-1.81</b>	0.66	0.29	-1.05	<b>1.73</b>	0.37	0.10	0.67
(j) 900 hPa stability (10 <sup>-3</sup> K m <sup>-1</sup> )	0.84	<b>3.23</b>	<b>-2.28</b>	-1.40	<b>3.42</b>	-1.22	1.15	<b>2.88</b>	<b>-2.08</b>
(k) CAPE (J kg <sup>-1</sup> )	23	-72	132	-40	-190	83	-9	-188	178

north of the urban area, especially in regions north of 40°N. In contrast, the increase in aerosols causes significant cooling from  $-0.6^{\circ}$  to  $-1.0^{\circ}$ C in central China and SC and some warming in the region to the northeast of China near 50°N (Fig. 3c). When combined (Fig. 3e), the aerosol cooling dominates, still resulting in significant cooling up to  $-0.4^{\circ}$ C in SC while the cooling in central China and NC is largely offset by the urban-induced warming. The significant cooling pattern in SC simulated with the combined urban and aerosol effect agrees well with the observed cooling pattern of  $0.2^{\circ}$ C decade<sup>-1</sup> during 1969–2000 that is concentrated around the YRV (Xu et al. 2006).

Changes in precipitation show a common southern flood and northern drought pattern owing to the increases in urban land use and/or aerosols (Figs. 3b,d,f). The urbanization results in a precipitation reduction between 28° and 41°N in a band oriented northeast to southwest but a precipitation increase in southeastern China (Fig. 3b). In comparison, the aerosol-induced precipitation reduction occurs farther north, along the YRB and covering northern and northeastern China, while significant precipitation increases are seen farther

south, along the coast of southeastern China (Fig. 3d). The combined urban and aerosol effect shows that precipitation reduction occurs in parts of northern and southwestern China up to  $1.2$  mm day<sup>-1</sup> (Fig. 3f). In contrast, precipitation increases of about  $0.8$  mm day<sup>-1</sup> are seen over southern China and the South China Sea (Fig. 3f).

### c. AOD, cloud, and radiation changes

Changes of summer-mean AOD and total cloud-cover fraction during 1993–2007 between the control experiment and the sensitivity experiments are shown in Fig. 4. Urbanization causes little change in AOD over EC (Fig. 4a), but a large decrease of  $\sim 1.8\%$  in total cloud cover over NC and an area north of China (northeastern China not included) [Fig. 4b and Table 3, row (e1)]. In contrast, urbanization induces a large increase of  $\sim 1.1\%$  in total cloud cover over a zone south of the YRV, with the largest increases around the southeast coast and the South China Sea (Fig. 4b). The increases over SC and the decreases over NC and Mongolia in cloud cover (Fig. 4b) suggest a circulation change induced by the urban effect. This is elucidated in section 4. Corresponding to the pattern of cloudiness changes, shortwave radiation for

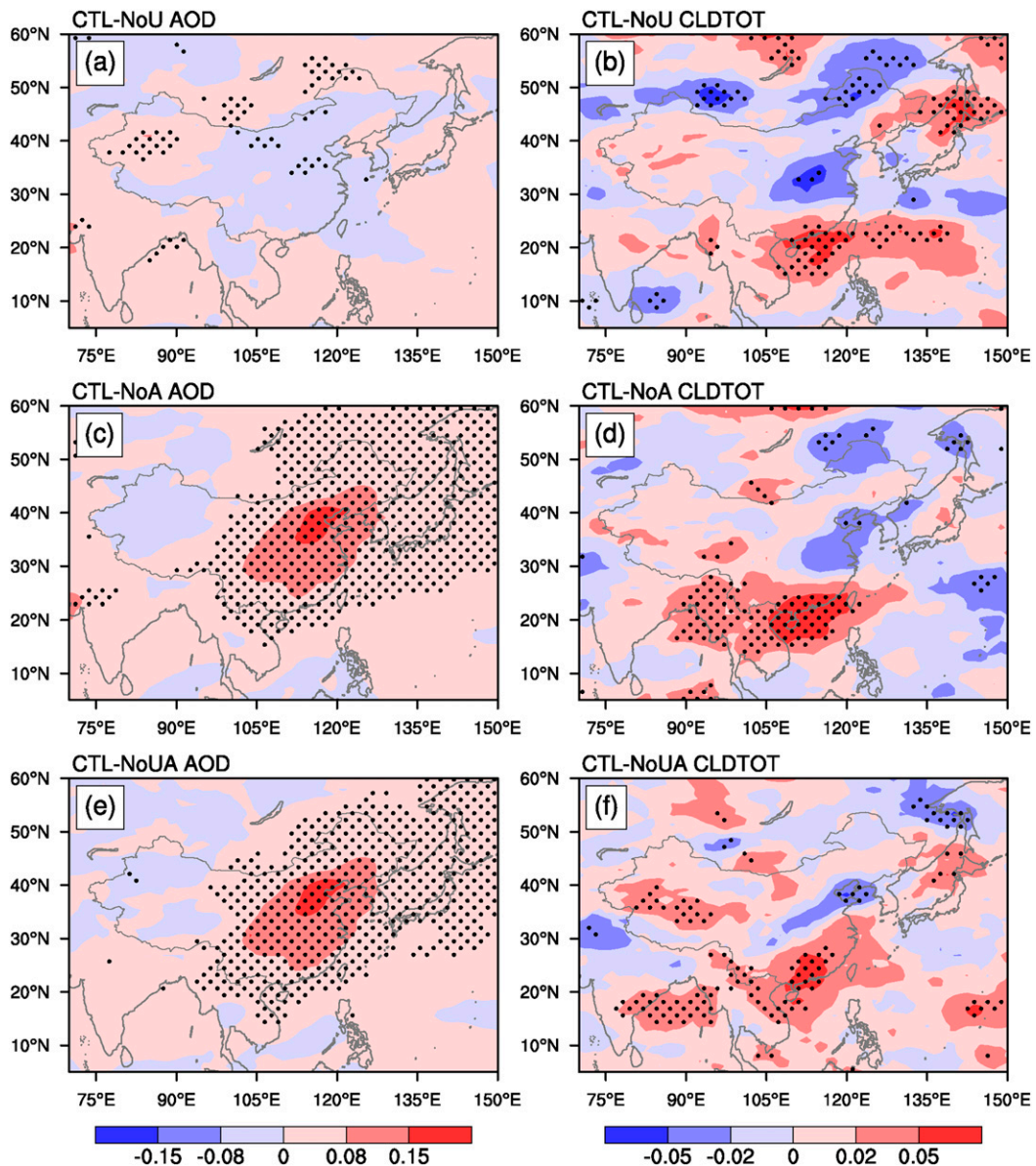


FIG. 4. Changes of the summer (left) AOD and (right) total cloud-cover fraction for (a),(b) CTL - NoU; (c),(d) CTL - 2NoA; and (e),(f) CTL - NoUA. The dotted areas are statistically significant at the 10% level.

all sky shows a significant increase in NC by about  $3.9 \text{ W m}^{-2}$  [Table 3, row (f4)] but a decrease in SC by  $5\text{--}15 \text{ W m}^{-2}$ , while shortwave radiation for clear sky shows a nonsignificant increase in NC.

The aerosol increase causes a significant increase in AOD by  $\sim 0.09$  in EC, particularly in NC with an increase of  $\sim 0.10$  [Table 3, row (d), and Fig. 4c]. The AOD increase leads to a significant reduction of about  $-7.4 \text{ W m}^{-2}$  in shortwave radiation for clear sky over all of East Asia, especially over NC by about  $-8.4 \text{ W m}^{-2}$  [Fig. 5c and Table 3, row (f3)]. The increase in aerosols causes a significant increase of total

cloud cover of about 2.6% in SC but a slight reduction in NC and eastern Mongolia (Fig. 4d). The opposite changes in cloud cover between SC and NC owing to the aerosol effect imply a possible change in atmospheric circulation, which is discussed in section 4. Combining the aerosols' direct effect on radiation and indirect effect on clouds, shortwave radiation for all sky shows a significant reduction in EC by  $-15.1 \text{ W m}^{-2}$ , particularly in SC by  $-20.2 \text{ W m}^{-2}$  [Fig. 5d and Table 3, row (f3)].

When both the urbanization and aerosol increases are included, the effects are not a linear combination of their individual effects. While changes in the AOD and

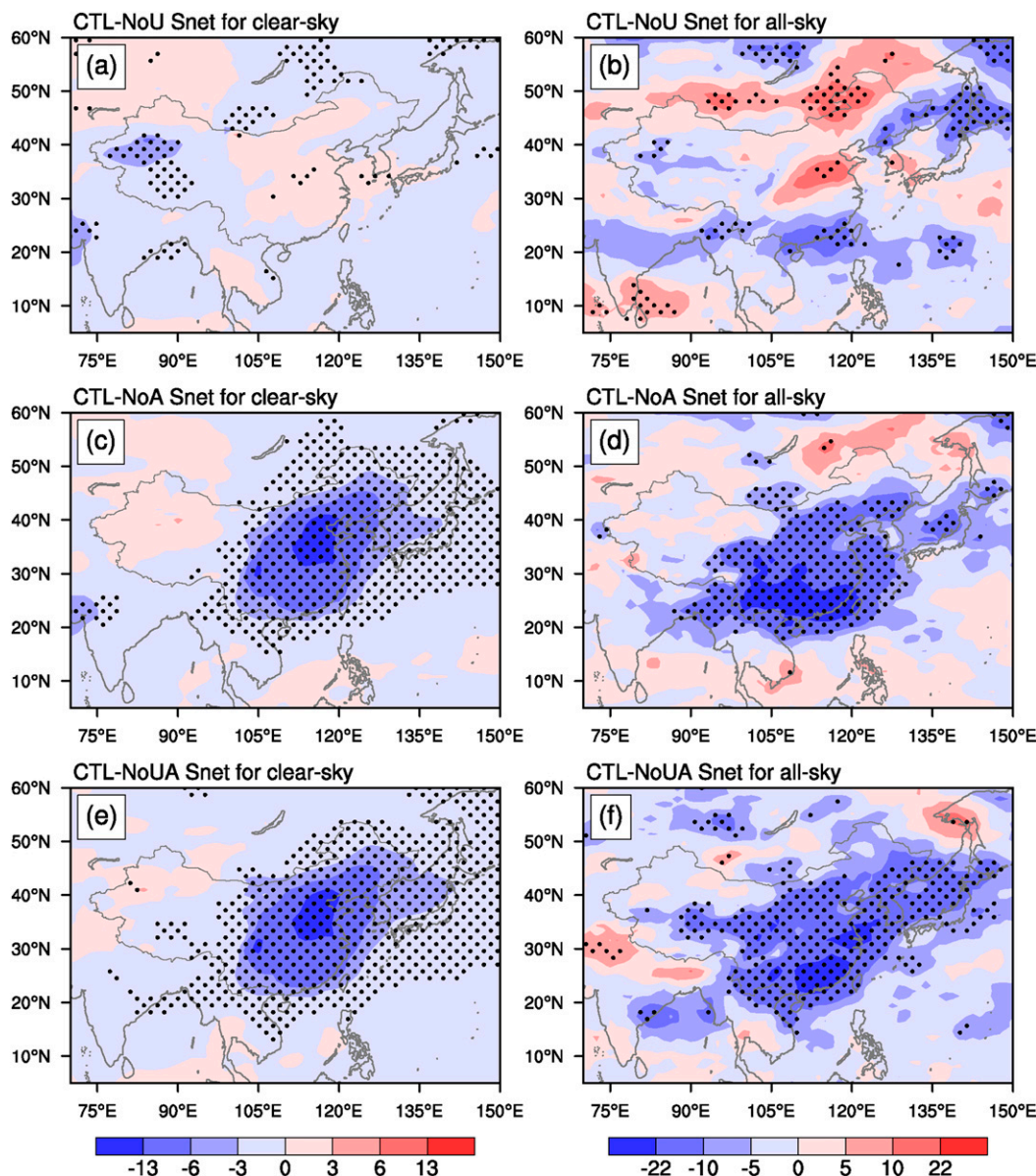


FIG. 5. Changes of the summer surface net shortwave radiation ( $W m^{-2}$ ) for (left) clear sky and (right) all sky for (a),(b) CTL - NoU; (c),(d) CTL - NoA; and (e),(f) CTL - NoUA. The dotted areas are statistically significant at the 10% level.

clear-sky shortwave radiation in the combined forcings are nearly the same as those in the aerosol-only case (Figs. 4c,e and 5c,e), changes in clouds and all-sky shortwave radiation are different from the aerosol-only case (Figs. 4b,d,f and 5d,f). The reductions in high and total clouds over NC in the CTL - NoUA case are smaller than both the CTL - NoU and CTL - NoA cases [Table 3, rows (e1) and (e2)], with areas of total cloud reduction shifted northward along the Yellow River region (Fig. 4f). In the meantime, the cloudiness increase over SC is also shifted northward closer to the YRV, implying

nonlinearity in the effects of the combined urban and aerosol forcings. As a result, all-sky shortwave radiation shows significant reductions of  $-10.6$  and  $-17.6 W m^{-2}$  over NC and SC, respectively (Fig. 5f), and they are dominated by aerosols' direct radiative effect over NC but by increased cloudiness over SC. These changes in cloudiness and all-sky shortwave radiation for CTL - NoUA are broadly like those for the CTL - NoA case, with larger decreases in all-sky shortwave radiation over SC than over NC. This contributes to the strong cooling centered in SC (Fig. 3e). Thus, the effect of the aerosol

forcing (large surface cooling) dominates over that of the urban forcing (moderate surface warming) in the combined case.

#### 4. Physical mechanisms and discussion

The above analysis of the effects of the urban and aerosol forcings on surface temperature and energy budgets suggests a need to better understand the thermal and dynamic processes responsible for the regional climate change, particularly for the opposite cloud-cover changes between NC and SC.

##### a. Impact of urban land-use changes

The results of the CTL show that air over East Asia is warmer than that over the surrounding oceans in summer, with the warmest over about 30°N in EC and decreasing temperature northward and southward of 30°N (Fig. 2). The southerly component of the monsoon winds that carries abundant water vapor prevails in the mid-to-lower troposphere over EC, and it weakens as the wind travels northward but extends all the way to about 45°N. Vertical–meridional profiles of summer circulation, relative humidity, and specific humidity in CTL (Fig. 6a) indicate that moist deep convection is dominant over the EASM area, causing strong ascent south of 40°N. The ascent over the region is accompanied by high specific humidity up to  $16 \text{ g kg}^{-1}$  in the lower troposphere. Under these background climatological conditions, the causes of the changes in atmospheric thermal properties and circulation characteristics are investigated below.

Urban land use, including anthropogenic heat, causes heating in the surface boundary layer, which results in elevating isobaric surfaces and wind divergence anomalies above the lower troposphere over urban areas. These thermodynamic processes are confirmed by the result of Chen et al. (2016), which demonstrated that large-scale urbanization over East Asia can cause increased geopotential height throughout the troposphere above 850 hPa over East Asia in June as the direct atmospheric response to the surface thermal forcing induced by the urbanization. In addition, urban surfaces reduce wind speed because of increased frictional drag (Changnon et al. 1981; Oke 1987; Thielen et al. 2000; Shao et al. 2013). Combining the wind speed reduction (due to its dynamic effect; Fig. 6b) with the increased divergence above 850 hPa in urban agglomeration areas between 30° and 40°N (due to the urban thermal effect; Fig. 6c), a convergence anomaly is initiated in SC, favoring ascending and more cloud cover. Latent heating from the increased ascent heats up the mid-to-upper troposphere over SC, which in turn reinforces surface convergence over SC (Fig. 6c). These thermodynamic

processes are also confirmed by results of Hoskins (1991) and Liu et al. (2004), which suggest that diabatic heating induces lower-layer cyclonic circulation and upper-layer anticyclonic circulation. Therefore, an enhanced ascent and increased cloud cover occur near 20°N, which causes an anomalous divergence at the upper troposphere over SC and northward advection and descent between 30° and 50°N (Fig. 6c). The anomalous descent around 30°N reduces the mean upward motion associated with deep convection shown in the climatology (Fig. 6a). The cooling anomaly over 30°N is the result of reduced latent heating due to the suppressed convection and the reduced longwave radiative heating because decreases in water vapor allow more longwave radiation to escape to space. These two cooling processes over 30°N are partially offset by the adiabatic warming from descending anomalies.

To further investigate the effect of urban land use on the atmosphere, the CTL – NoU differences of the vertical–meridional profiles of temperature, relative humidity, and specific humidity averaged over 105°–122°E are examined (Fig. 6d). Significant increases in temperature (due to urban heat island effect plus other effects discussed below) and decreases in near-surface specific humidity [due to impervious urban surfaces and thus reduced evaporation; Table 3, row (c3)] in the urban areas between 30° and 40°N cause a reduction in near-surface relative humidity in this region that also extends throughout the troposphere (Fig. 6d). The reduced surface moisture shown in the urban agglomeration areas is consistent with the results of Feng et al. (2015). To examine whether the increased surface heating and reduced evaporation in urban areas affect the stability and the large-scale circulation, changes in summer equivalent potential temperature gradient  $\partial\theta_e/\partial z$  at 900 hPa and convective available potential energy (CAPE) for CTL – NoU are shown in Table 3, rows (j) and (k). It is found that  $\partial\theta_e/\partial z$  increases and CAPE decreases over the agglomerate urban region (30°–40°N) and NC [Table 3, rows (j) and (k)]. Thus, the atmosphere becomes more stable, which suppresses atmospheric deep convection in this region (30°–40°N). In contrast, decreases of  $\partial\theta_e/\partial z$  and increases of CAPE occur over SC [Table 3, rows (j) and (k)], which corresponds to enhanced moisture convergence in the lower troposphere south of 30°N (Fig. 6c). Thus, the increased instability and enhanced moisture convergence favor cloud formation and convection over SC and a cyclonic anomaly around 15°–25°N in the lower troposphere (Fig. 6b).

To diagnose the adiabatic heating or cooling,  $\omega(RT/c_p - \partial T/\partial p)$  (where  $T$  is the temperature,  $\omega$  is the vertical pressure velocity,  $c_p$  is the specific heat at constant

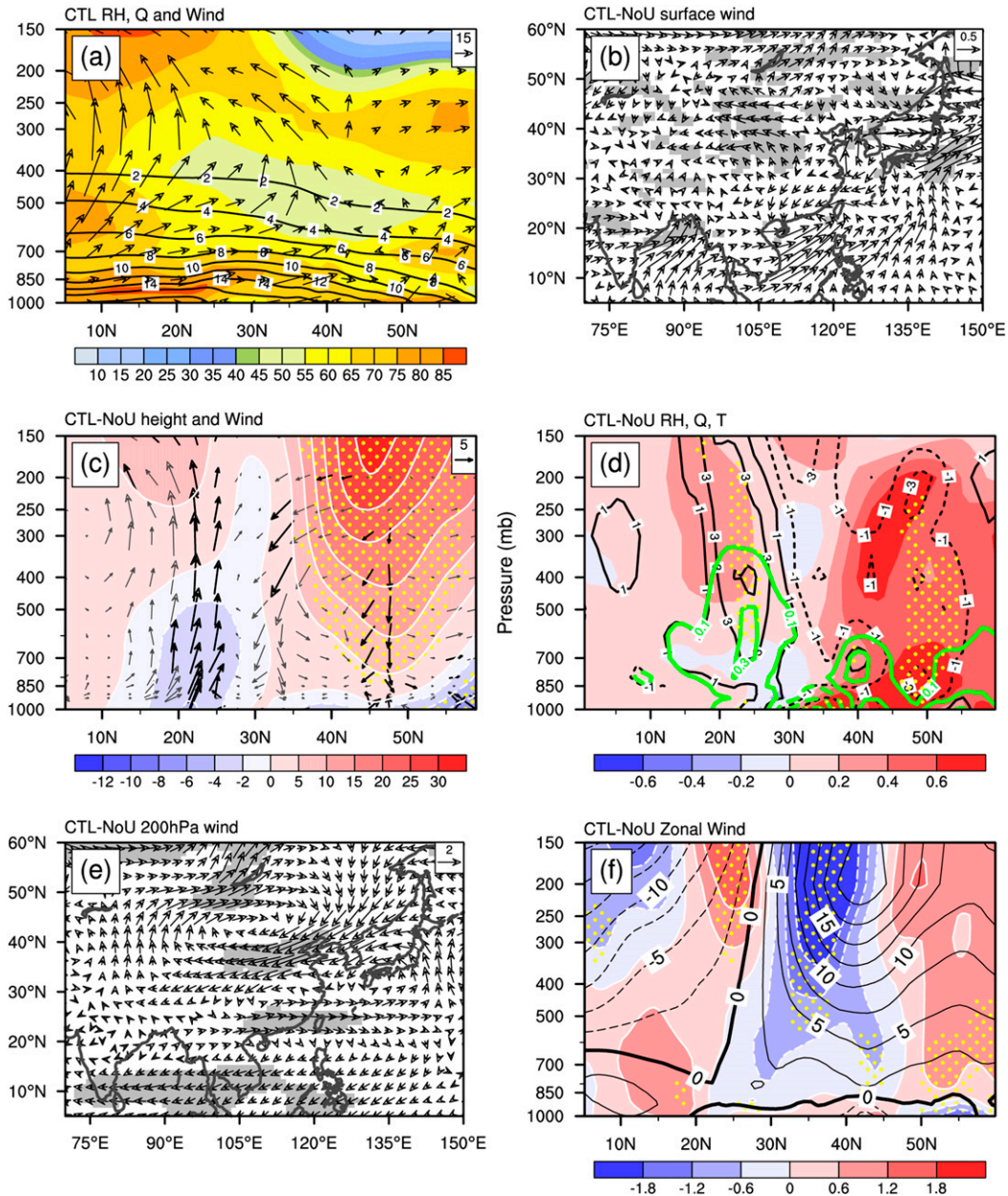


FIG. 6. (a) Vertical-meridional profiles of summer relative humidity (%; color shading), specific humidity ( $\text{g kg}^{-1}$ ; contours), and winds (vectors) averaged over  $105^{\circ}\text{--}122^{\circ}\text{E}$  in CTL. The winds depicted are the  $v$ - $\omega$  components, where  $v$  ( $\text{m s}^{-1}$ ) is meridional velocity and  $-\omega$  ( $10^{-3} \text{ Pa s}^{-1}$ ) is vertical pressure velocity (positive upward). (b) The CTL - NoU difference of the summer surface winds ( $\text{m s}^{-1}$ ). The shaded areas are statistically significant at the 10% level. (c) The CTL - NoU difference of the summer vertical-meridional profiles of geopotential height (gpm; color) and circulation (arrows), all averaged over  $105^{\circ}\text{--}122^{\circ}\text{E}$ , depicted as for the winds in (a); the black thick arrows are statistically significant at the 10% level for vertical pressure velocity; the dotted areas are statistically significant at the 10% level for geopotential height. (d) The CTL - NoU difference of the vertical-meridional profiles of summer relative humidity (%; black contours), specific humidity ( $\text{g kg}^{-1}$ ; thick green contours), and temperature ( $^{\circ}\text{C}$ ; color) averaged over  $105^{\circ}\text{--}122^{\circ}\text{E}$ . The dotted areas are statistically significant at the 10% level for relative humidity. (e) The CTL - NoU difference of the summer horizontal winds ( $\text{m s}^{-1}$ ) at 200 hPa, with the shaded areas being statistically significant at the 10% level. (f) The CTL - NoU difference of the summer vertical-meridional profiles of zonal wind ( $\text{m s}^{-1}$ ; color; contours indicate zonal wind in CTL), all averaged over  $105^{\circ}\text{--}122^{\circ}\text{E}$ . The dotted areas are statistically significant at the 10% level for the colored field.

pressure,  $p$  is the pressure, and  $R$  is the gas constant) was calculated following Holton (1992). Accompanying the anomalous descent north of about 35°N, positive adiabatic heating up to  $0.9 \text{ K day}^{-1}$  occurs in the troposphere (figures not shown), which contributes to the anomalous warming throughout the whole troposphere at those latitudes (Fig. 6d). The anomalous heating elevates isobaric surfaces in the troposphere, which leads to an anticyclonic anomaly over central Mongolia (Fig. 6e). To the west and northwest of the anticyclonic anomaly, the anomalous southerly flow also increases the warm advection to the north of 50°N in the troposphere, contributing to the warming throughout the troposphere over a large region north and west of the urban region and over NC (Figs. 3a and 6d). Because of the heating anomaly north of 30°N, meridional temperature gradients between 25° and 45°N decrease greatly in the troposphere, which causes easterly wind anomalies that weaken the westerly winds at these latitudes over EC (Fig. 6f). The easterly wind anomaly in the upper troposphere, accompanied by the anomalous descending flows around 40°N and the warm advection to the west and northwest of the descent, reinforces the formation of the anticyclonic anomaly at 200 hPa centered over Mongolia (Fig. 6e).

The strong anticyclonic anomaly suppresses cloud formation over north and northeastern China, leading to a reduction in low, high, and total cloud amounts over these regions [Table 3, rows (e1)–(e3), and Fig. 4b]. Over NC, the decreases in cloudiness significantly increase surface net radiation and sensible heat flux by  $6.1$  and  $2.5 \text{ W m}^{-2}$ , respectively, which contributes to the enhanced surface warming over NC in addition to the direct warming resulting from the urban heat island, anthropogenic heat, and reduced surface evaporation [Table 3, rows (c2) and (f4), and Fig. 3a]. In regions farther north and west of the urban areas, increases in shortwave radiation due to reduced cloudiness also contribute to the temperature increase in addition to the warm advection. Further, longwave radiation loss to space is increased in these regions due to the reduced water vapor content, but its cooling effect is relatively small in comparison with the diabatic heating from the increased shortwave radiation, the adiabatic heating due to the increased descending, and the horizontal warm air advection (figures not shown). These thermal and dynamic processes initiated by urban land use lead to a significant anticyclonic anomaly (Figs. 6c,e), which in turn maintains feedbacks to these heating processes.

To the south of the anomalous anticyclone centered over Mongolia, a northeasterly anomaly occurs over north and northeastern China throughout the troposphere, and it further enhances convergence and

cyclonic anomaly in the lower troposphere along the coast of SC (centered at 23°N, 115°E). Therefore, over EC, the northeasterly wind anomaly, which is caused concurrently by the anticyclonic anomaly north of 40°N and the cyclonic anomaly south of 30°N, weakens the southwesterly monsoon flow. These results are consistent with the responses of the late summer monsoon circulation due to urban land use simulated by Chen et al. (2016), who showed a high-level anticyclonic anomaly over NC and a low-level cyclonic anomaly over the South China Sea.

### b. Impact of anthropogenic aerosols

Changes in cloud cover shown in Fig. 4d and Table 3, rows (e1) and (e3), suggest circulation changes induced by anthropogenic aerosols. Vertical–meridional profiles of summer temperature and circulation averaged over 105°–122°E and horizontal winds at the lower and upper troposphere for CTL – NoA are examined in detail to understand the thermodynamic processes involved (Fig. 7). Aerosols cause strong cooling between 25° and 40°N in the whole troposphere, with two notable cooling centers. One is at the surface and lower troposphere between 25° and 35°N, and the other one is at 300 hPa above 35°N. The reduction in air temperature between 25° and 35°N in the lower troposphere exceeds  $0.6^\circ\text{C}$ . The scattering of solar radiation by sulfate aerosols reduces surface solar radiation (Fig. 5c) and thus cools the surface and the lower troposphere, as suggested by Jiang et al. (2013). The regionally averaged reductions of shortwave radiation for clear sky and all sky over EC are  $-7.4$  and  $-15.1 \text{ W m}^{-2}$ , respectively [Table 3, rows (f3) and (f4)]. The aerosol-induced cooling over East Asia (Fig. 3c) reduces the summer land–sea thermal contrast and increases the pressure in the lower troposphere as well as at the sea level over EC [Table 3, row (g)]. This decreases the horizontal pressure gradient force between land and ocean, which weakens southwesterly monsoon winds.

The large tropospheric cooling between 25° and 40°N increases the meridional temperature gradient south of 30°N, which causes westerly wind anomalies between 20° and 30°N in the mid-to-upper troposphere (Fig. 7b). This enhances the subtropical westerly jet stream and increases baroclinic instability over SC. In contrast, the cooling anomalies reduce the meridional temperature gradient between 35° and 50°N, which causes easterly wind anomalies at these latitudes in the mid-to-upper troposphere, weakens the westerly jet stream, and reduces baroclinic instability over NC.

On the other hand, surface and tropospheric cooling between 25° and 40°N leads to the depressed isobaric surfaces in the mid-to-upper troposphere, which favors

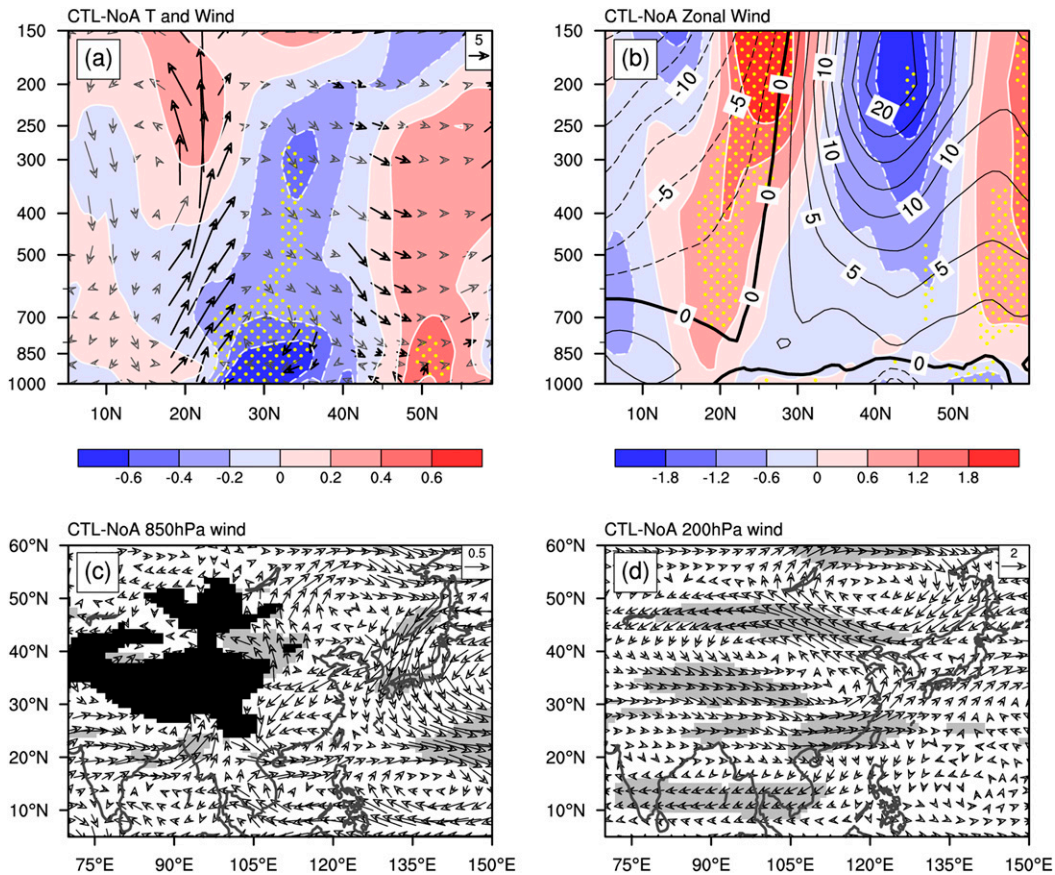


FIG. 7. The CTL – NoA difference of the summer vertical-meridional profiles of (a) temperature ( $^{\circ}\text{C}$ ; color) and circulation (arrows), all averaged over  $105^{\circ}\text{--}122^{\circ}\text{E}$ , depicted as in Fig. 6c, and (b) zonal wind ( $\text{m s}^{-1}$ ; color; contours indicate zonal wind in CTL), all averaged over  $105^{\circ}\text{--}122^{\circ}\text{E}$ . The dotted areas are statistically significant at the 10% level for the colored field; the thick black arrows are statistically significant at the 10% level for vertical pressure velocity. The CTL – NoA difference of the summer horizontal winds ( $\text{m s}^{-1}$ ) at (c) 850 and (d) 200 hPa, with the shaded areas being statistically significant at the 10% level.

the formation of the cyclonic anomaly, as is shown most clearly at 200 hPa (Fig. 7d). The anomalous southeasterly flow to the northeast of the cyclonic anomaly increases the warm advection between  $40^{\circ}$  and  $50^{\circ}\text{N}$ , which partially offsets aerosol-induced cooling over NC and even causes anomalous warming over northeastern China around  $50^{\circ}\text{N}$  (Figs. 3c and 7a). The anomalous warming elevates isobaric surfaces in the troposphere, which leads to an anticyclonic anomaly in the upper troposphere over northeastern China (Fig. 7d).

The reduced southwesterly monsoon winds north of  $25^{\circ}\text{N}$  favor moisture convergence and significant ascent around  $20^{\circ}\text{N}$  (Fig. 7a), thus leading to increases in cloud cover and latent heating in the mid-to-upper troposphere. The latent heating in turn enhances surface convergence and ascent through the thermodynamic feedback. Thus, a cyclonic anomaly occurs along the coast of southern China ( $20^{\circ}\text{N}$ ,  $115^{\circ}\text{E}$ ; Fig. 7c). The enhanced baroclinicity

and convergence both produce a favorable condition for deep convection and precipitation over SC (Fig. 3d). Therefore, anthropogenic aerosols reduce shortwave radiation not only by direct scattering but also through the weakened monsoon flow to enhance convergence and cloud cover over SC, especially low clouds. Both of these effects significantly reduce all-sky shortwave radiation over SC [Fig. 5d and Table 3, row (f4)]. At the same time, the northward moisture transport to northern and northeastern China is reduced because of the weakened southwesterly monsoon flow north of  $25^{\circ}\text{N}$  and the enhanced moisture convergence over the coast of SC. Thus, over NC, reduced moisture convergence and baroclinic instability decrease cloud cover, which partially offsets shortwave radiation reduction by the aerosols' direct cooling effect [Fig. 5d and Table 3, row (f4)] and lessens the reduction in all-sky shortwave radiation. Combining the aerosols' direct cooling effect, centered in NC

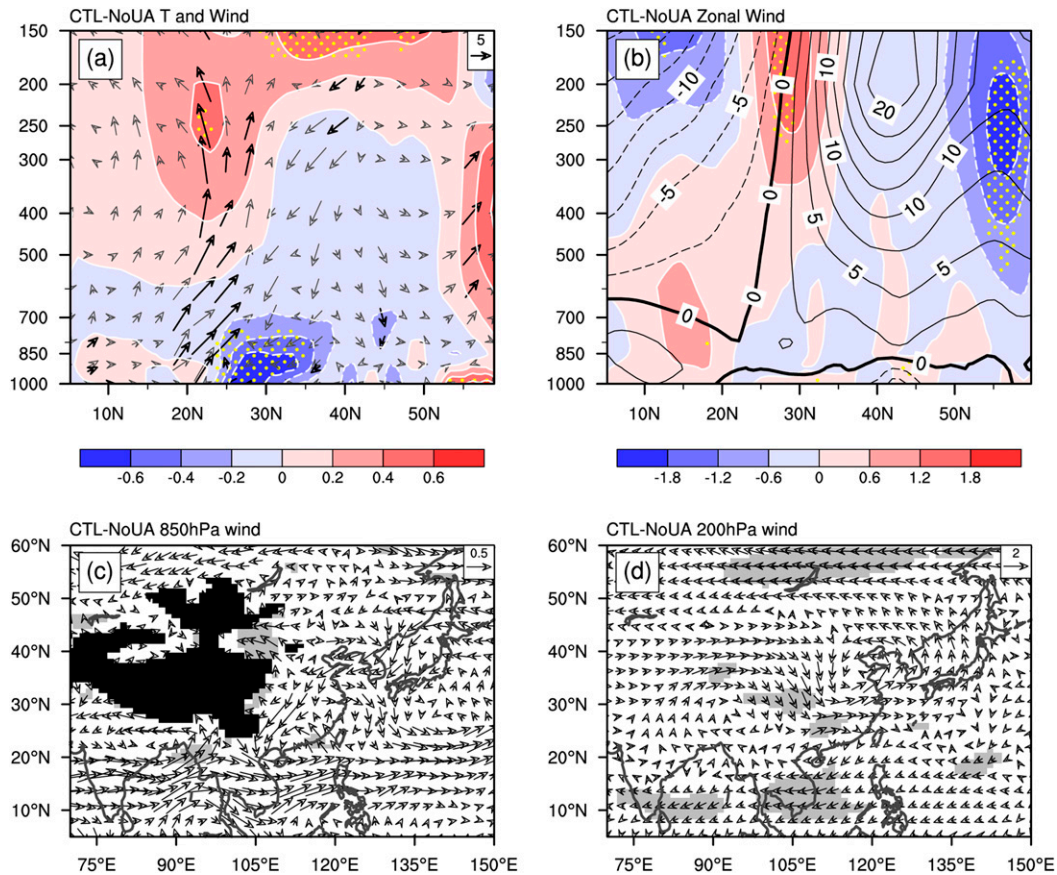


FIG. 8. As in Fig. 7, but for the CTL-NoA case.

(Figs. 4c and 5c), and the cloud cooling effect induced by the circulation change, centered along the coast of southern China (Fig. 4d), the largest cooling occurs over SC where the two cooling effects overlap (Fig. 3c). The weakened EASM in response to aerosols and a cyclonic anomaly over the coast of SC are in agreement with the results of Jiang et al. (2013) and Song et al. (2014), although temperature changes here differ from these studies.

### c. Joint impact of urbanization and aerosols

In the combined case CTL – NoUA, changes at the surface (Fig. 3e) and in the troposphere (Fig. 8) differ substantially from the two individual forcing cases. Significant cooling occurs south of 30°N at the surface and in the lower troposphere, and weak cooling extends to the mid-to-upper troposphere between about 30° and 50°N (Fig. 8a). The cooling magnitude of the combined urban and aerosol effects is smaller than the aerosol-only case. Therefore, the reduction in the land–ocean thermal contrast during the EASM is less than that caused by aerosols only. Nevertheless, the weakened southwesterly monsoon winds north of 25°N still

favor convergence and ascent over SC although the vertical motion anomaly is reduced (Figs. 7a and 8a). The warming in the mid-to-upper troposphere around 20°N (Fig. 8a), which is caused by latent heating with anomalous ascent, further enhances convergence and a cyclonic circulation anomaly in the lower troposphere but divergence in the upper troposphere over SC (Figs. 8a,c). These temperature changes increase the meridional temperature gradient around 30°N and cause westerly wind anomalies between 20° and 30°N in the mid-to-upper troposphere (Fig. 8b), thus enhancing the subtropical westerly jet stream and increasing baroclinic instability over SC. Corresponding to the anomalous surface convergence and baroclinicity, the increase in cloudiness dominates the cooling at the surface and in the lower troposphere over SC (Figs. 3e and 8a).

When urban and aerosol effects are both considered, the aerosols' cooling effect is partially offset by the urban effect, and the increase in sea level pressure caused by aerosols in EC is reduced greatly [Table 3, row (g)]. Further, the cyclonic anomaly developed in the mid-to-upper troposphere is weak in comparison with the aerosol

case (Figs. 7d and 8d). The anomalous descending over NC, which is forced by the enhanced upper-tropospheric divergence over SC, together with the weakened southwesterly monsoon winds and the increased frictional drag in EC, decreases cloud cover [Fig. 4f and Table 3, row (e1)]. Thus, large cooling is located in SC when both urban and aerosol effects are considered (Figs. 3e and 8a). In comparison with the widespread cooling over EC in the aerosol-only case (Figs. 3c and 7a), the cooling pattern for the combined case is much closer to the surface temperature trends over China from station observations for the last three decades (Xu et al. 2006). Moreover, the enhanced cooling in SC at the surface and in the lower troposphere helps maintain a northeasterly anomaly over EC through thermal wind relationship and thus a weakened EASM and wetter and drier conditions in SC and NC, respectively.

In summary, the cooling effect of the increased anthropogenic aerosols dominates in the combined case, and it is partly offset by the urban-induced warming at the surface and in the troposphere north of about 35°N. Thus, the cooling magnitude in the combined case is much smaller than aerosol-only case. The effects of urbanization and anthropogenic aerosols on air temperature, clouds, and precipitation are found to be a nonlinear combination of the effects from these two components separately. Further studies on the nonlinearity between the two individual components are needed.

## 5. Summary and conclusions

Surface and atmospheric responses to the increased urban land use and anthropogenic aerosol emissions since the preindustrial era in China are investigated both individually and jointly using a comprehensive atmospheric model (i.e., CAM5.1). This model can simulate aerosols' direct and indirect effects and is coupled with a physically based urban module. The physical mechanisms that help maintain the circulation anomalies are found to either amplify the direct effects of urbanization or aerosols when their effects are considered separately or reduce them through their nonlinear interactions when their effects are jointly considered. The urban land use in EC, including anthropogenic heat, induces a large warming at the surface, which elevates isobaric surfaces and increases wind divergence above 850 hPa over the urban region. The urban surface reduces wind speed because of increased frictional drag. Combining the divergence with the wind speed reduction, a convergence anomaly is initiated in SC, favoring ascent, cloud formation, and increased latent heating, which further enhances surface convergence and upper-level divergence over SC. This causes enhanced northward advection in

the upper troposphere and descent between 30° and 50°N. The anomalous descent north of 30°N not only reduces cloud cover and increases surface solar heating but also contributes to an anomalous warming in the troposphere at those latitudes by adiabatic heating, which in turn further elevates isobaric surfaces in the troposphere and leads to an anticyclonic anomaly over central Mongolia. To the west and northwest of the anticyclonic anomaly, anomalous southerly flows also contribute to the tropospheric heating by warm advection to the north of 50°N. Consequently, westerly winds over midlatitude East Asia are reduced significantly, particularly in the mid-to-upper troposphere, associated with reduced meridional thermal gradients.

Anthropogenic aerosols decrease surface shortwave radiation over most of East Asia by directly reflecting and absorbing solar radiation in the atmosphere, thus causing widespread cooling over most East Asia, including both NC and SC. This cooling reduces the summer land–sea thermal contrast and increases the pressure in the lower troposphere over EC. The decrease in the horizontal pressure gradient force between land and ocean weakens southwesterly monsoon winds over EC. The reduced southwesterly winds favor moisture convergence and ascent around 20°N, thus leading to increases in cloud formation and latent heating in the mid-to-upper troposphere over SC. The latent heating in turn enhances not only surface convergence and ascent over SC but also divergence in the upper troposphere. Thus, anomalous northward airflow and forced descent north of 30°N occur in response to the thermal and dynamic adjustment over SC. This reduces cloud cover over NC. On the other hand, surface and tropospheric cooling between 25° and 40°N over EC leads to depressed isobaric surfaces in the mid-to-upper troposphere, which favors the formation of the cyclonic anomaly in the upper troposphere. To the northeast of the cyclonic anomaly, anomalous warm advection between 40° and 50°N partially offsets aerosol induced cooling over NC and even causes anomalous warming over northeastern China.

When the urban and aerosol effects are combined, circulation changes induced by aerosols' cooling effect are partially offset by the urban heating effect, especially north of 30°N. Nevertheless, their joint effect still leads to weakening of the EASM circulation but at reduced magnitude in comparison with the aerosols' effect. Thus, although the anomalous ascending and descending still occur over SC and NC, respectively, the aforementioned pattern of cloudiness changes is shifted northward with significant cooling areas confined to SC.

The model-simulated effects of urbanization and aerosols over eastern China are qualitatively consistent

with the weakening in the EASM circulation since the 1960s (e.g., [Gong and Ho 2002](#); [Yu et al. 2004](#); [Ding et al. 2008](#); [Li et al. 2010](#)), although recent studies ([Zhu et al. 2011, 2015](#); [Xu et al. 2015](#)) suggest that the EASM has restrengthened since about 1999, associated with recent decadal SST changes in the Pacific. This seems to suggest a more dominant role of Pacific SSTs ([Li et al. 2010](#)) than the effects of urbanization and aerosols, especially the role of the PDO or the IPO, which apparently switched from a positive to negative phase around 1999 ([Dai 2013](#); [Dong and Dai 2015](#); [Zhu et al. 2015](#)). Because of the complexity in the physical mechanisms between urbanization/aerosols and EASM and deficiencies of the model, uncertainties likely remain in the simulated results discussed here. To reduce the uncertainties, ensemble simulations with different initial states are necessary to reduce the effect of internal variability. Model simulations longer than 20 yr would make the result more robust. In addition, coupled atmosphere and ocean modeling could capture ocean response to the atmospheric circulation change instead of prescribed SST. Therefore, further studies are still needed in the future to reduce uncertainties and make the result more robust.

*Acknowledgments.* This project is funded by the National Key Basic Research Program (973 Program) of China under Grant 2010CB428505, the National Key Research and Development Program of China (Grant 2016YFA0600402), and a Project Funded by the Priority Academic Program Development (PAPD) of Jiangsu Higher Education Institutions. Model experiments were conducted using computer resources at the National Center for Atmospheric Research (NCAR). A. Dai is supported by the U.S. National Science Foundation (Grant AGS-1353740), the U.S. Department of Energy's Office of Science (Award DE-SC0012602), and the U.S. National Oceanic and Atmospheric Administration (Award NA15OAR4310086).

## REFERENCES

- Adler, R. F., and Coauthors, 2003: The Version-2 Global Precipitation Climatology Project (GPCP) monthly precipitation analysis (1979–present). *J. Hydrometeorol.*, **4**, 1147–1167, doi:[10.1175/1525-7541\(2003\)004<1147:TVGPCP>2.0.CO;2](#).
- Albrecht, B. A., 1989: Aerosols, cloud microphysics, and fractional cloudiness. *Science*, **245**, 1227–1230, doi:[10.1126/science.245.4923.1227](#).
- Bollasina, M. A., Y. Ming, and V. Ramaswamy, 2011: Anthropogenic aerosols and the weakening of the South Asian summer monsoon. *Science*, **334**, 502–505, doi:[10.1126/science.1204994](#).
- Boucher, O., and Coauthors, 2013: Clouds and aerosols. *Climate Change 2013: The Physical Science Basis*, T. F. Stocker et al., Eds., Cambridge University Press, 571–657.
- Bretherton, C. S., M. Widmann, V. P. Dymnikov, J. M. Wallace, and I. Bladé, 1999: The effective number of spatial degrees of freedom of a time-varying field. *J. Climate*, **12**, 1990–2009, doi:[10.1175/1520-0442\(1999\)012<1990:TENOSD>2.0.CO;2](#).
- Changnon, S. A., Jr., 1978: Urban effects on severe local storms at St. Louis. *J. Appl. Meteor.*, **17**, 578–586, doi:[10.1175/1520-0450\(1978\)017<0578:UEOSLS>2.0.CO;2](#).
- , R. G. Semonin, A. H. Auer, R. R. Braham, and J. Hales, 1981: *METROMEX: A Review and Summary*. Meteor. Monogr., No. 40, Amer. Meteor. Soc., 81 pp.
- Charlson, R. J., S. Schwartz, J. Hales, R. D. Cess, J. Coakley Jr., J. Hansen, and D. Hofmann, 1992: Climate forcing by anthropogenic aerosols. *Science*, **255**, 423–430, doi:[10.1126/science.255.5043.423](#).
- Chen, H. S., and Y. Zhang, 2013: Sensitivity experiments of impacts of large-scale urbanization in east China on East Asian winter monsoon. *Chin. Sci. Bull.*, **58**, 809–815, doi:[10.1007/s11434-012-5579-z](#).
- , —, M. Yu, W. Hua, S. Sun, X. Li, and C. Gao, 2016: Large-scale urbanization effects on eastern Asian summer monsoon circulation and climate. *Climate Dyn.*, **47**, 117–136, doi:[10.1007/s00382-015-2827-3](#).
- Dai, A., 2013: The influence of the inter-decadal Pacific oscillation on U.S. precipitation during 1923–2010. *Climate Dyn.*, **41**, 633–646, doi:[10.1007/s00382-012-1446-5](#).
- , H. Li, Y. Sun, L. C. Hong, LinHo, C. Chou, and T. Zhou, 2013: The relative roles of upper and lower tropospheric thermal contrasts and tropical influences in driving Asian summer monsoons. *J. Geophys. Res. Atmos.*, **118**, 7024–7045, doi:[10.1002/2013JC009297](#).
- Dai, Y. F., Y. M. Liu, and L. J. Zhou, 2011: Observational analysis of urbanization effect on surface air temperature trends in east China (in Chinese). *J. Meteor. Sci.*, **31**, 365–371.
- Dee, D. P., and Coauthors, 2011: The ERA-Interim reanalysis: Configuration and performance of the data assimilation system. *Quart. J. Roy. Meteor. Soc.*, **137**, 553–597, doi:[10.1002/qj.828](#).
- Deng, J., and H. Xu, 2015: Atmospheric responses to idealized urban land surface forcing in eastern China during the boreal spring. *J. Geophys. Res. Atmos.*, **120**, 10 022–10 039, doi:[10.1002/2015JD023748](#).
- Ding, Y., Z. Wang, and Y. Sun, 2008: Inter-decadal variation of the summer precipitation in east China and its association with decreasing Asian summer monsoon. Part I: Observed evidences. *Int. J. Climatol.*, **28**, 1139–1161, doi:[10.1002/joc.1615](#).
- , Y. Sun, Z. Wang, Y. Zhu, and Y. Song, 2009: Inter-decadal variation of the summer precipitation in China and its association with decreasing Asian summer monsoon. Part II: Possible causes. *Int. J. Climatol.*, **29**, 1926–1944, doi:[10.1002/joc.1759](#).
- , Y. J. Liu, Y. F. Song, and J. Zhang, 2015: From MONEX to the global monsoon: A review of monsoon system research. *Adv. Atmos. Sci.*, **32**, 10–31, doi:[10.1007/s00376-014-0008-7](#).
- Dong, B., and A. Dai, 2015: The influence of the inter-decadal Pacific oscillation on temperature and precipitation over the globe. *Climate Dyn.*, **45**, 2667–2681, doi:[10.1007/s00382-015-2500-x](#).
- Feddema, J. J., K. W. Oleson, G. B. Bonan, L. O. Mearns, L. E. Buja, G. A. Meehl, and W. M. Washington, 2005: The importance of land-cover change in simulating future climates. *Science*, **310**, 1674–1678, doi:[10.1126/science.1118160](#).

- Feng, J. M., Y. L. Wang, and Z. G. Ma, 2015: Long-term simulation of large-scale urbanization effect on the East Asian monsoon. *Climatic Change*, **129**, 511–523, doi:10.1007/s10584-013-0885-2.
- Findell, K. L., E. Shevliakova, P. Milly, and R. J. Stouffer, 2007: Modeled impact of anthropogenic land cover change on climate. *J. Climate*, **20**, 3621–3634, doi:10.1175/JCLI4185.1.
- Gong, D. Y., and C. H. Ho, 2002: Shift in the summer rainfall over the Yangtze River valley in the late 1970s. *Geophys. Res. Lett.*, **29**, 1436, doi:10.1029/2001GL014523.
- Harris, I., P. Jones, T. Osborn, and D. Lister, 2014: Updated high-resolution grids of monthly climatic observations—The CRU TS3.10 dataset. *Int. J. Climatol.*, **34**, 623–642, doi:10.1002/joc.3711.
- Holton, J. R., 1992: *An Introduction to Dynamic Meteorology*. 3rd ed. Academic Press, 54 pp.
- Hoskins, B. J., 1991: Towards a PV- $\theta$  view of the general circulation. *Tellus*, **43A**, 27–35, doi:10.1034/j.1600-0870.1991.t01-3-00005.x.
- Huffman, G. J., R. F. Adler, D. T. Bolvin, and G. Gu, 2009: Improving the global precipitation record: GPCP version 2.1. *Geophys. Res. Lett.*, **36**, L17808, doi:10.1029/2009GL040000.
- Hurrell, J., J. Hark, D. Shea, J. Caron, and J. Rosinski, 2008: A new sea surface temperature and sea ice boundary dataset for the Community Atmosphere Model. *J. Climate*, **21**, 5145–5153, doi:10.1175/2008JCLI2292.1.
- Jackson, T. L., J. J. Feddema, K. W. Oleson, G. B. Bonan, and J. T. Bauer, 2010: Parameterization of urban characteristics for global climate modeling. *Annu. Assoc. Amer. Geogr.*, **100**, 848–865, doi:10.1080/00045608.2010.497328.
- Jiang, Y., X. Liu, X. Q. Yang, and M. Wang, 2013: A numerical study of the effect of different aerosol types on East Asian summer clouds and precipitation. *Atmos. Environ.*, **70**, 51–63, doi:10.1016/j.atmosenv.2012.12.039.
- Jones, P. D., D. H. Lister, and Q. X. Li, 2008: Urbanization effects in large-scale temperature records: With an emphasis on China. *J. Geophys. Res.*, **113**, D16122, doi:10.1029/2008JD009916.
- Kalnay, E., and M. Cai, 2003: Impact of urbanization and land-use change on climate. *Nature*, **423**, 528–531, doi:10.1038/nature01675.
- Kaufmann, R. K., K. C. Seto, A. Schneider, Z. T. Liu, L. Zhou, and W. Wang, 2007: Climate response to rapid urban growth: Evidence of a human-induced precipitation deficit. *J. Climate*, **20**, 2299–2306, doi:10.1175/JCLI4109.1.
- Kishtawal, C. M., D. Niyogi, M. Tewari, R. A. Pielke, and J. M. Shepherd, 2010: Urbanization signature in the observed heavy rainfall climatology over India. *Int. J. Climatol.*, **30**, 1908–1916, doi:10.1002/joc.2044.
- Lamarque, J. F., and Coauthors, 2010: Historical (1850–2000) gridded anthropogenic and biomass burning emissions of reactive gases and aerosols: Methodology and application. *Atmos. Chem. Phys.*, **10**, 7017–7039, doi:10.5194/acp-10-7017-2010.
- Lawrence, P. J., and T. N. Chase, 2010: Investigating the climate impacts of global land cover change in the community climate system model (CCSM). *Int. J. Climatol.*, **30**, 2066–2087, doi:10.1002/joc.2061.
- Li, H., A. Dai, T. Zhou, and J. Lu, 2010: Responses of East Asian summer monsoon to historical SST and atmospheric forcing during 1950–2000. *Climate Dyn.*, **34**, 501–514, doi:10.1007/s00382-008-0482-7.
- Li, Z., 2004: Aerosol and climate: A perspective from East Asia. *Observation, Theory and Modeling of Atmospheric Variability*, X. Zhu, Ed., World Scientific, 501–525.
- , and Z. Yan, 2009: Homogenized daily mean/maximum/minimum temperature series for China from 1960–2008. *Atmos. Ocean. Sci. Lett.*, **2**, 237–243, doi:10.1080/16742834.2009.11446802.
- Liu, X., and Coauthors, 2012: Toward a minimal representation of aerosols in climate models: description and evaluation in the Community Atmosphere Model CAM5. *Geosci. Model Dev.*, **5**, 709–739, doi:10.5194/gmd-5-709-2012.
- Liu, Y., G. Wu, and R. Ren, 2004: Relationship between the subtropical anticyclone and diabatic heating. *J. Climate*, **17**, 682–698, doi:10.1175/1520-0442(2004)017<0682:RBTSAA>2.0.CO;2.
- Lohmann, U., and J. Feichter, 2005: Global indirect aerosol effects: A review. *Atmos. Chem. Phys.*, **5**, 715–737, doi:10.5194/acp-5-715-2005.
- Ma, H., Z. Jiang, J. Song, A. Dai, X. Yang, and F. Huo, 2016: Effects of urban land-use change in east China on the East Asian summer monsoon based on the CAM5.1 model. *Climate Dyn.*, **46**, 2977–2989, doi:10.1007/s00382-015-2745-4.
- Miyakoda, K., J. Kinter III, and S. Yang, 2003: The role of ENSO in the South Asian monsoon and premonsoon signals over the Tibetan Plateau. *J. Meteor. Soc. Japan*, **81**, 1015–1039, doi:10.2151/jmsj.81.1015.
- National Bureau of Statistics of China, 2014: *China Statistical Yearbook*. China Statistics Press. [Available online at <http://www.stats.gov.cn/tjsj/ndsj/2014/indexeh.htm>.]
- Neale, R. B., and Coauthors, 2012: Description of the NCAR Community Atmospheric Model (CAM5.0). NCAR Tech. Note NCAR/TN-486+STR, 289 pp. [Available online at [http://www.cesm.ucar.edu/models/cesm1.0/cam/docs/description/cam5\\_desc.pdf](http://www.cesm.ucar.edu/models/cesm1.0/cam/docs/description/cam5_desc.pdf).]
- Ohara, T., H. Akimoto, J. Kurokawa, N. Horii, K. Yamaji, X. Yan, and T. Hayasaka, 2007: An Asian emission inventory of anthropogenic emission sources for the period 1980–2020. *Atmos. Chem. Phys.*, **7**, 4419–4444, doi:10.5194/acp-7-4419-2007.
- Oke, T. R., 1987: *Boundary Layer Climates*. 2nd ed. Routledge, 435 pp.
- Oleson, K. W., G. B. Bonan, J. Feddema, and M. Vertenstein, 2008: An urban parameterization for a global climate model. Part II: Sensitivity to input parameters and the simulated urban heat island in offline simulations. *J. Appl. Meteor. Climatol.*, **47**, 1061–1076, doi:10.1175/2007JAMC1598.1.
- , —, —, —, and E. Kluzek, 2010a: Technical description of an urban parameterization for the Community Land Model (CLMU). NCAR Tech. Note NCAR/TN-480+STR, 178 pp., doi:10.5065/D6K35RM9.
- , and Coauthors, 2010b: Technical description of version 4.0 of the Community Land Model (CLM). NCAR Tech. Note NCAR/TN-478+STR, 266 pp. [Available online at [http://www.cesm.ucar.edu/models/cesm1.0/clm/CLM4\\_Tech\\_Note.pdf](http://www.cesm.ucar.edu/models/cesm1.0/clm/CLM4_Tech_Note.pdf).]
- Pielke, R. A., Sr., 2005: Land use and climate change. *Science*, **310**, 1625–1626, doi:10.1126/science.1120529.
- Rosenfeld, D., U. Lohmann, G. B. Raga, C. D. O’Dowd, M. Kulmala, S. Fuzzi, A. Reissell, and M. O. Andreae, 2008: Flood or drought: How do aerosols affect precipitation? *Science*, **321**, 1309–1313, doi:10.1126/science.1160606.
- Shao, H., J. Song, and H. Ma, 2013: Sensitivity of the East Asian summer monsoon circulation and precipitation to an idealized large-scale urban expansion. *J. Meteor. Soc. Japan*, **91**, 163–177, doi:10.2151/jmsj.2013-205.

- Shepherd, J. M., H. Pierce, and A. J. Negri, 2002: Rainfall modification by major urban areas: Observations from spaceborne rain radar on the TRMM satellite. *J. Appl. Meteor.*, **41**, 689–701, doi:10.1175/1520-0450(2002)041<0689:RMBMUA>2.0.CO;2.
- Smith, S. J., J. van Aardenne, Z. Klimont, R. J. Andres, A. Volke, and S. Delgado Arias, 2011: Anthropogenic sulfur dioxide emissions: 1850–2005. *Atmos. Chem. Phys.*, **11**, 1101–1116, doi:10.5194/acp-11-1101-2011.
- Song, F., T. Zhou, and Y. Qian, 2014: Responses of East Asian summer monsoon to natural and anthropogenic forcings in the 17 latest CMIP5 models. *Geophys. Res. Lett.*, **41**, 596–603, doi:10.1002/2013GL058705.
- Song, X., G. J. Zhang, and J.-L. Li, 2012: Evaluation of microphysics parameterization for convective clouds in the NCAR Community Atmosphere Model CAM5. *J. Climate*, **25**, 8568–8590, doi:10.1175/JCLI-D-11-00563.1.
- Streets, D., and Coauthors, 2003: An inventory of gaseous and primary aerosol emissions in Asia in the year 2000. *J. Geophys. Res.*, **108**, 8809, doi:10.1029/2002JD003093.
- Sun, Y., Y. Ding, and A. Dai, 2010: Changing links between South Asian summer monsoon circulation and tropospheric land-sea thermal contrasts under a warming scenario. *Geophys. Res. Lett.*, **37**, L02704, doi:10.1029/2009GL041662.
- Thielen, J., W. Wobrock, A. Gadian, P. G. Mestayer, and J. D. Creutin, 2000: The possible influence of urban surfaces on rainfall development: A sensitivity study in 2D in the meso-gamma scale. *Atmos. Res.*, **54**, 15–39, doi:10.1016/S0169-8095(00)00041-7.
- U.S. Energy Information Administration, 2012: China. U.S. Energy Information Administration Rep., 36 pp. [Available online at [http://www.eia.gov/beta/international/analysis\\_includes/countries\\_long/China/china.pdf](http://www.eia.gov/beta/international/analysis_includes/countries_long/China/china.pdf).]
- Wan, H., and Z. Zhong, 2014: Ensemble simulations to investigate the impact of large-scale urbanization on precipitation in the lower reaches of Yangtze River valley, China. *Quart. J. Roy. Meteor. Soc.*, **140**, 258–266, doi:10.1002/qj.2125.
- Wang, C., 2013: Impact of anthropogenic absorbing aerosols on clouds and precipitation: A review of recent progresses. *Atmos. Res.*, **122**, 237–249, doi:10.1016/j.atmosres.2012.11.005.
- Wang, X., 2010: Urbanization path and city scale in China: An economic analysis (in Chinese). *Econ. Res. J.*, **10**, 20–32.
- Wang, Y., and Coauthors, 2011: Seasonal variations in aerosol optical properties over China. *J. Geophys. Res.*, **116**, D18209, doi:10.1029/2010JD015376.
- Wu, G., and Coauthors, 2016: Advances in studying interactions between aerosols and monsoon in China. *Sci. China Earth Sci.*, **59**, 1–16, doi:10.1007/s11430-015-5198-z.
- Xie, Z. Q., Y. Du, Y. Zeng, Y. Shi, and J. Wu, 2007: Impact of urbanization on regional temperature change in the Yangtze River delta. *Acta Meteor. Sin.*, **62**, 717–727.
- Xu, M., C. P. Chang, C. Fu, Y. Qi, A. Robock, D. Robinson, and H. Zhang, 2006: Steady decline of East Asian monsoon winds, 1969–2000: Evidence from direct ground measurements of wind speed. *J. Geophys. Res.*, **111**, D24111, doi:10.1029/2006JD007337.
- Xu, Q., 2001: Abrupt change of the mid-summer climate in central east China by the influence of atmospheric pollution. *Atmos. Environ.*, **35**, 5029–5040, doi:10.1016/S1352-2310(01)00315-6.
- Xu, Z., K. Fan, and H. Wang, 2015: Decadal variation of summer precipitation over China and associated atmospheric circulation after the late 1990s. *J. Climate*, **28**, 4086–4108, doi:10.1175/JCLI-D-14-00464.1.
- Yang, S., and K. Lau, 2006: Interannual variability of the Asian Monsoon. *The Asian Monsoon*, B. Wang, Ed., Praxis Publishing, 259–293.
- Yu, R., B. Wang, and T. Zhou, 2004: Tropospheric cooling and summer monsoon weakening trend over East Asia. *Geophys. Res. Lett.*, **31**, 217–244, doi:10.1029/2003GL018471.
- , J. Li, Y. Zhang, and H. Chen, 2015: Improvement of rainfall simulation on the steep edge of the Tibetan Plateau by using a finite-difference transport scheme in CAM5. *Climate Dyn.*, **45**, 2937–2948, doi:10.1007/s00382-015-2515-3.
- Zhang, D. L., Y. X. Shou, and R. E. Dickerson, 2009: Upstream urbanization exacerbates urban heat island effects. *Geophys. Res. Lett.*, **36**, L24401, doi:10.1029/2009GL041082.
- Zhou, L., Z. Jiang, Z. Li, and X. Yang, 2015: Numerical simulation of urbanization climate effects in regions of east China (in Chinese). *Chin. J. Atmos. Sci.*, **39**, 596–610.
- Zhou, L. M., R. E. Dickinson, Y. H. Tian, J. Fang, Q. Li, R. Kaufmann, C. Tucker, and R. Myneni, 2004: Evidence for a significant urbanization effect on climate in China. *Proc. Natl. Acad. Sci. USA*, **101**, 9540–9544, doi:10.1073/pnas.0400357101.
- Zhu, Y., H. Wang, W. Zhou, and J. Ma, 2011: Recent changes in the summer precipitation pattern in East China and the background circulation. *Climate Dyn.*, **36**, 1463–1473, doi:10.1007/s00382-010-0852-9.
- , —, J. Ma, T. Wang, and J. Sun, 2015: Contribution of the phase transition of Pacific decadal oscillation to the late 1990s' shift in east China summer rainfall. *J. Geophys. Res. Atmos.*, **120**, 8817–8827, doi:10.1002/2015JD023545.